

1
2
3
4
5 **Neural mechanisms of social learning in the female mouse**

6 Yuan Gao¹, Carl Budlong¹, Emily Durlacher², and Ian G. Davison^{1,*}

7 ¹ Department of Biology, Boston University, Boston MA 02215

8 ² Program in Neuroscience and Behavior, Mt. Holyoke College, South Hadley MA
9 01075

10
11 * Corresponding author: Ian Davison

12 Email: idavison@bu.edu
13
14

15 **Conflict of interest:** The authors declare no competing financial interests.
16

17 **Acknowledgments:** We thank members of the Davison laboratory, Yoram Ben-Shaul,
18 Tim Gardner, Adi Mizrahi, Jennifer Morgan, and Stephen Shea for comments and
19 discussion. This work was supported by the Klingenstein Foundation, the Binational
20 Science Foundation, and NIH/NIDCD (R21DC013894).

Summary

Social interactions are often powerful drivers of learning. In female mice, mating creates a long-lasting sensory memory for the pheromones of the stud male that alters neuroendocrine responses to his chemosignals for many weeks. The cellular and synaptic correlates of pheromonal learning, however, remain unclear. We examined local circuit changes in the accessory olfactory bulb (AOB) using targeted *ex vivo* recordings of mating-activated neurons tagged with a fluorescent reporter. Imprinting led to striking plasticity in the intrinsic membrane excitability of projection neurons (mitral cells, MCs) that dramatically curtailed their responsiveness, suggesting a novel cellular substrate for pheromonal learning. Plasticity selectively targeted the MC ensembles activated by the stud male, consistent with formation of memories for specific individuals. Finally, MC excitability gained atypical activity-dependence whose slow dynamics strongly attenuated firing on timescales of several minutes. This unusual form of AOB plasticity may act to filter sustained or repetitive sensory signals.

Introduction

Chemical cues detected by the vomeronasal system convey vital social information, influencing diverse behaviors such as reproduction (Bruce and Parrott, 1960; Kimchi et al., 2007), pair bonding (Young and Wang, 2004), parental care (Dulac et al., 2014; Kendrick et al., 1992; Levy et al., 2004), individual recognition (Hurst, 2009), and aggression (Chamero et al., 2007; Stowers et al., 2002b). Vomeronasal pathways directly access the limbic system, consistent with their powerful role in guiding behavior, and also influence neuroendocrine centers to modify physiological and hormonal status (Dulac and Torello, 2003; Tirindelli et al., 2009).

While vomeronasal circuits often elicit stereotyped behavioral and neuroendocrine responses, they can also be highly plastic. In one striking example, female mice imprint on the pheromones of the stud male after mating, where a single salient sensory experience drives long-term changes in both behavior and the flow of sensory information to central targets (Keverne and Brennan, 1996). During the first few days after fertilization, chemosignals from unfamiliar males typically block pregnancy by altering the female's neuroendocrine state (Bruce and Parrott, 1960). However, mating opens a plasticity window that creates a recognition memory for the stud's pheromones, so that they lose their potency and no longer disrupt embryo implantation (Brennan and Keverne, 1997). Memories are formed within hours, yet last weeks or longer (Kaba and Keverne, 1988). Sensory imprinting thus offers an opportunity to test the neural basis of a natural form of social learning in a circuit intimately coupled with intraspecies behaviors.

While social experience acts on diverse neural circuits throughout the brain (Wallace et al., 2009; Wu et al., 2014), mating-dependent learning is strongly linked to plasticity in the accessory olfactory bulb (AOB). Imprinting in females leads to local neurochemical changes (Brennan et al., 1995), is affected by local lesions or pharmacological interventions (Brennan and Keverne, 1997; Kaba et al., 1994; Kaba and Keverne, 1988), and can be artificially induced by manipulating AOB signaling (Kaba et al., 1994). Pheromonal cues are encoded in AOB by the firing of mitral cells (MCs), whose activity signals gender, hormonal status, and in particular, strain and/or individual identity (Ben-Shaul et al., 2010; Luo et al., 2003; Tolokh et al., 2013). Well-established theories propose that learning selectively suppresses the firing of the MCs encoding the stud male so that his pheromones no longer drive neuroendocrine responses, precluding pregnancy block (Brennan, 2004; Brennan et al., 1990). MC suppression is further proposed to depend on strengthening of local inhibitory circuits in AOB, consisting largely of granule cells (GCs) that supply feedback inhibition to MCs through unique dendrodendritic synapses (Isaacson and Strowbridge, 1998; Shepherd and Greer, 1998). Inhibitory plasticity is consistent with both microdialysis data (Brennan and Binns, 2005; Brennan et al., 1995) and ultrastructural changes in local interneurons (Matsuoka et al., 1997; Matsuoka et al., 2004).

Despite well-established models of learning in AOB, many key features of plasticity remain untested. To date, direct measurements of either synaptic plasticity or changes in MC output are lacking. Furthermore, while the selectivity of recognition memories for different individual or strains is thought to rely on plasticity in specific groups of MC, there are no data linking plasticity to functionally defined cell populations.

More broadly, the nature of the neural changes that allow for adaptive changes in social behavior remain poorly understood.

Here, we examined how mating affects local AOB microcircuits using targeted whole-cell recordings of identified neurons activated by the stud male in *ex vivo* brain slices. We found pronounced reductions in the sensitivity of AOB neurons, which unexpectedly were mediated by changes in intrinsic excitability rather than synaptic strength, suggesting a novel cellular basis for encoding sensory memories in AOB. MC firing was selectively attenuated in stud-activated neurons, suggesting a potential basis for the specificity of pheromonal learning. Changes in MC responsiveness emerged only when they were activated with repetitive patterns, suggesting that after learning the AOB may dynamically filter repetitive sensory signals from the stud male, lessening their impact on neuroendocrine status on long timescales.

Results

Slow, powerful self-inhibition in AOB MCs

While inhibitory circuits are intensively studied in main olfactory bulb (Isaacson and Strowbridge, 1998; Shepherd and Greer, 1998), their role in shaping AOB output is not well characterized. We thus began by characterizing self-inhibition in AOB projection neurons, mitral cells (MCs). MC self-inhibition arises from specialized dendrodendritic synapses shared with local interneurons, primarily granule cells (GCs) (Figure 1A). We assessed self-inhibition by driving MC firing with current injection and examining the resulting synaptic feedback from interneurons. Brief, high-frequency spike trains

generated only modest feedback inhibition in AOB (Figures 1B-C), comparable but smaller on average than reported in main olfactory bulb (Abraham et al., 2010; Margrie et al., 2001). However, pronounced inhibition appeared when we drove MCs with prolonged stimuli similar in duration to chemosensory responses, which can last for tens of seconds (Luo et al., 2003). Extended MC spike trains elicited slowly emerging but robust barrages of inhibitory postsynaptic potentials (IPSPs) that contributed to a strong decline in firing rate (Figures 1D – 1F; Figure 1 – source data 1). In contrast, the same protocol generated little detectable inhibition in MCs of the main olfactory bulb, where high firing rates were sustained throughout the train. To confirm that synaptic self-inhibition shapes MC output, we eliminated dendrodendritic feedback pathways by blocking fast synaptic transmission with NBQX, APV, and gabazine (5, 25, and 10 μ M respectively). Pharmacologically eliminating feedback inhibition typically increased MC firing as well (Figure 1 – figure supplement 1). Together, our results suggest that MC self-inhibition is substantially stronger in AOB than in main olfactory bulb, but also unusually slow to manifest, consistent with the prolonged sensory responses characteristic of this brain area. Such powerful self-inhibition by single MCs could potentially provide a basis for cell-specific control over AOB output, as previously proposed (Brennan and Keverne, 1997).

Mating enhances synaptic inhibition in AOB

Microdialysis suggests increased bulk GABA release in AOB after mating (Brennan and Binns, 2005), consistent with enhanced inhibition, but the synaptic correlates of

imprinting have not been measured directly. We next examined the effects of pheromonal learning on local inhibitory circuits. To align the timing of mating with brain slice recordings (Figure 2A), we induced estrus using ovariectomy, implanted estradiol capsules, and progesterone injection (Strom et al., 2012). We then paired females in their home cage with sexually experienced males for 4 hours to provide the mating and sensory exposure required for imprinting. Females engaged in frequent, repetitive investigation of males, particularly of facial and anogenital regions (Figure 2 – figure supplement 1A-C; mean interval, 62.1 ± 7.99 sec; median, 15.9 sec). Investigative behavior was elevated in mated relative to sensory-exposed females, suggesting that they experienced both heightened arousal states and increased levels of sensory input during the pairing period (Figure 2 – figure supplement 1D).

Immediately following mating and sensory exposure, we prepared AOB brain slices from females and examined changes in synaptic inhibition with whole-cell voltage-clamp recordings of MCs. We compared three groups: (i) mating plus sensory experience with a freely moving male; (ii) sensory-exposed controls without mating; and (iii) naïve mice with no prior male exposure, housed overnight in a fresh cage. We measured GABAergic input onto MCs by recording miniature inhibitory postsynaptic currents (mIPSCs; Figure 2B). IPSCs were pharmacologically isolated with 5 μ M NBQX, 25 μ M APV, and 1 μ M TTX (Figure 2 – figure supplement 2). The frequency of mIPSCs was strongly increased in mated animals vs. naïve and sensory-exposed groups (Figures 2C-D; 2.45 ± 0.37 Hz vs. 1.48 ± 0.21 Hz and 1.28 ± 0.17 Hz respectively). The mean amplitude of mIPSCs was similar for all three conditions, suggesting little change in the postsynaptic sensitivity of inhibitory synapses onto MCs (Figures 2E-F; 56.8 ± 3.5

pA, 54.5 ± 3.8 pA, and 65.8 ± 6.1 pA for naïve, sensory-exposed and mated mice respectively; Figure 2 – source data 1). The distribution of amplitudes was shifted towards higher values, however, indicating that a subset of inhibitory synapses may be strengthened. Overall, mating experience substantially increased inhibitory input onto MCs, consistent with prior microdialysis results (Brennan et al., 1995).

Because imprinting may act on other elements of the self-inhibition pathway, we also asked whether mating alters excitatory input to granule cells, the most numerous interneurons in AOB. Using current clamp recordings from GCs, we measured the amplitude and frequency of spontaneous excitatory postsynaptic potentials (sEPSPs; Figure 2G). The frequency of sEPSPs was elevated in mated relative to naïve and sensory-exposed females (Figures 2H-I; 4.25 ± 0.71 , 3.57 ± 0.56 , and 6.61 ± 0.63 Hz for naïve, exposure and mated groups respectively). EPSP amplitude was also slightly enhanced in mated compared to naïve animals (Figure 2J-K, 1.08 ± 0.08 , 1.18 ± 0.10 , and 1.44 ± 0.10 mV for naïve, exposed, and mated groups respectively). These differences were consistent across a wide range of EPSP detection criteria (Figure 2 – figure supplement 3). Overall, learning also increased excitatory drive onto GCs, enhancing both presynaptic and postsynaptic elements of glutamatergic synapses. Together, our data suggest that imprinting upregulates both the excitatory and inhibitory components of the pathways for MC self-inhibition.

Synaptic plasticity lacks cellular selectivity

168 Pheromonal recognition memories are specific to particular individuals or strains,
169 implying that learning may act selectively on the particular AOB neurons activated by
170 the stud's chemosignals (Keverne and Brennan, 1996). To test the cellular specificity of
171 plasticity, we identified the AOB neurons activated during mating and sensory exposure
172 using GFP reporter lines based on the promoters for the immediate-early genes *Arc* and
173 *Fos* (Reijmers et al., 2007; Wang et al., 2006). We then used fluorescence-guided
174 recordings (Barth, 2007) to evaluate cellular and synaptic changes specifically in the
175 neural population activated during mating.

176 We focused first on interneurons, which were robustly labeled in *Arc*-GFP
177 animals. Prior to recording, we assessed GFP labeling across the GC population with 2-
178 photon microscopy. Naïve animals showed low levels of background GFP expression
179 (Figure 3A), and 4 hours of sensory exposure to a male in the absence of mating
180 produced little additional labeling over background (Figure 3 - figure supplement 1A).
181 However, mating combined with subsequent sensory exposure drove strong GFP
182 expression in a subset of GCs, consistent with *Arc* immunolabeling in AOB in response
183 to conspecifics (Halem et al., 2001; Matsuoka et al., 2002). We found robust labeling in
184 both anterior and posterior AOB, consistent with prior reports using histochemical
185 staining (Brennan et al., 1992; Halem et al., 2001). Fluorescent activity reporters
186 therefore identify mating-activated neural populations in live AOB tissue for targeted *ex*
187 *vivo* electrophysiological measurements.

188 Using fluorescence-guided recordings of GFP-labeled GCs (Figure 3B), we
189 asked whether the synaptic plasticity generated by mating was specific to these
190 neurons. Unexpectedly, there was no difference between GFP(-) and GFP(+)

populations of GCs for either amplitude or frequency of spontaneous excitatory input (Figures 3C-D; amplitude, 1.43 ± 0.15 vs 1.48 ± 0.13 mV; frequency, 7.13 ± 0.98 vs. 6.41 ± 0.84 Hz for unlabeled and labeled cells respectively; Figure 3 – source data 1). Similarly, there was no significant relationship between the intensity of GFP expression and either amplitude or frequency of EPSPs (Figures 3E-F). These data suggest that mating globally increased synaptic drive onto inhibitory GCs without apparent specificity to the neurons activated by the stud male.

AOB output is relayed to behavioral and neuroendocrine centers by MCs, suggesting that memory specificity ultimately relies on changes in these neurons. Because MCs were only weakly labeled by Arc-GFP, we used an alternative Fos-GFP reporter line (Reijmers and Mayford, 2009). Fos-GFP levels were low in MCs from naïve females, but were robustly elevated in a subset of MCs after mating (Figure 3G; Figure 3 – figure supplement 1B). Fos-GFP also provided more extensive labeling of GCs, suggesting that it captured similar sets of activated neurons, but at a lower threshold. As with GCs, we found no systematic differences in MC labeling in anterior vs. posterior AOB. In mated females, approximately 28% of detected MCs were classified as GFP(+) (intensity 4X greater than neuropil), but this is likely an overestimate due to difficulty in detecting unlabeled cells with live tissue imaging.

To correlate inhibitory plasticity with activation of MCs by the stud male, we repeated our measurements of GABAergic input using fluorescence-guided recordings (Fig. 3H). This second dataset revealed a similar two-fold increase in mIPSC frequency in mated vs. naïve animals, with no change in amplitude (Figure 3 – figure supplements 1C-H; frequency, 0.86 ± 0.14 vs. 1.68 ± 0.17 Hz; amplitude, 58.02 ± 5.59 vs. $63.21 \pm$

5.53 pA for naïve vs. mated respectively). We evaluated the cellular specificity of synaptic changes within mated females by subdividing the second MC dataset into studied activated GFP(+) neurons and a corresponding GFP(-) population. Similar to interneuron results, there was no significant difference in mean amplitude and frequency of mIPSCs between GFP(-) and GFP(+) MCs (Figures 3I and 3J; amplitude, 65.98 ± 8.15 vs. 57.86 ± 3.15 pA for unlabeled and labeled cells respectively; frequency, 1.43 ± 0.18 vs. 1.83 ± 0.31 Hz). Furthermore, there was no apparent correlation between GFP levels and properties of mIPSCs (Figures 3K and 3L). However, we cannot exclude the possibility that a larger sample may have revealed differences. Together, these results further indicate that imprinting drives synaptic plasticity in AOB inhibitory circuits. In contrast with established learning models, however, synaptic changes were widely distributed across both GC and MC populations with no apparent relationship to activation during mating.

Mating enhances interneuron excitability

The lack of specificity in synaptic plasticity suggested that AOB output may be shaped by alternative mechanisms. One possibility is changes in intrinsic membrane excitability, which will alter the recruitment of AOB neurons by shifting the threshold for generating action potential firing. We tested for learning-induced changes in membrane excitability in AOB using graded current injections, focusing first on interneurons.

The responsiveness of GCs in Arc-GFP females was enhanced after mating, so that less current was needed to initiate firing, and higher firing rates were produced by

the same current steps (Figures 4A-B). Increased excitability was also reflected in depolarized GC resting potentials, which were shifted by nearly 10 mV in mated versus naïve animals (Figure 4C, -72.1 ± 1.6 , -71.0 ± 1.6 , and -66.3 ± 1.2 mV for naïve, exposed, and mated groups respectively). Other properties, such as membrane resistance and slope of the input-output firing function, were unchanged across groups (Figure 4D, $R_{\text{input}} = 469 \pm 35$ vs. 520 ± 34 for naïve and mated groups; $p = 0.31$; ANOVA with post-hoc Tukey test), suggesting that increased GC responsiveness was largely determined by resting potential. Overall, mating increased the intrinsic excitability of AOB interneurons, suggesting that synaptic plasticity in inhibitory circuits is complemented by additional non-synaptic mechanisms.

To test whether changes in excitability were specific to mating-activated GCs, we examined the relationship between resting potential and Arc-GFP labeling. As with synaptic measurements, GC resting potential was uncorrelated with GFP intensity (Figure 4E). Furthermore, when we subdivided the GC dataset from mated animals into GFP(-) and GFP(+) populations, mean resting potential was similar for the two groups (Figure 4F; -67.0 ± 2.2 vs. -65.4 ± 1.9 mV respectively; Figure 4 – source data 1). Together, the increased GC excitability after mating indicates that learning acts on intrinsic as well as synaptic properties of AOB neurons. However, intrinsic plasticity was widespread across interneurons, and lacked dependence on prior activation during mating.

Mating attenuates MC responsiveness to repetitive stimuli

Because information about strain and individual identity is ultimately conveyed by MCs (Arnson and Holy, 2013; Ben-Shaul et al., 2010; Luo et al., 2003), the effects of learning should ultimately be reflected in their firing patterns. To further evaluate mating-dependent changes in AOB output, we compared responses to current injection in MCs from naïve and mated female Arc-GFP mice. In both groups, MCs responded to current injection with robust firing that decayed during the step (Figure 5A). In contrast to GCs, however, mating had no apparent effect on MC responses to a single stimulus. We found no difference in peak firing rate, total spike count during the train, or decay of firing between naïve and mated females (Figures 5B-D; peak firing: 15.0 ± 3.0 Hz vs. 17.4 ± 1.8 Hz; total spike count: 153 ± 28 vs. 176 ± 25 for naïve vs. mated respectively; Figure 5 – source data 1). Despite robust increases in inhibitory input, therefore, MC firing for a single stimulus was unchanged.

Although immediate effects on MC output were not apparent, we further probed for changes over longer time periods. The hormonal changes that induce pregnancy block require prolonged AOB activity lasting several hours (Li et al., 1994; Rosser et al., 1989), timescales that typically encompass multiple sensory interactions (Hull and Dominguez, 2007). To approximate repeated activation of vomeronasal inputs (see Figure 2 figure supplement 1), we probed MCs with repetitive stimuli spanning several minutes (ten current injections, 20 sec in duration, repeated every 60 sec). Surprisingly, in mated females MC firing often declined dramatically across successive trials, so that even neurons initially responding with hundreds of action potentials ceased firing entirely (Figure 5E). While firing also declined in some neurons from naïve animals, MC attenuation was greatly enhanced after imprinting, so that average spike counts in

mated females dropped to less than half than that of controls (Figures 5F-G; 80 ± 11 % vs. $36 \pm 8\%$). Together, our data indicate that mating leads to an unusual form of plasticity in MC membrane properties, where firing gains a striking dependence on recent history of activity. This metaplasticity in intrinsic excitability offers an alternative mechanism for attenuating AOB output, dramatically suppressing MC firing to repetitive stimuli and curtailing their responsiveness on timescales of minutes.

Changes in excitability are specific to stud-activated MCs

To account for individual-specific recognition memories, AOB plasticity is predicted to be expressed selectively in the MC ensemble activated by the stud. Because targeted MC recordings were precluded by weak labeling in Arc-GFP mice, we tested for selective changes in excitability by collecting a second dataset using the Fos-GFP reporter. Within mated females, we compared responses of labeled MCs with unlabeled cells that presumably represent other, non-stud chemosignals. Mating drove robust increases in Fos-GFP relative to sensory-exposed controls, generating detectable labeling in approximately 25% of MCs (Figure 3 – figure supplement 1B). After mating, both labeled and unlabeled MCs fired similarly to initial stimuli, consistent with Arc-GFP results (Figures 6A-D; peak firing rate, 15.2 ± 3.2 Hz vs. 16.2 ± 2.4 Hz; total spike count, 155 ± 39 vs. 133 ± 26 for GFP(-) and GFP(+) respectively; Figure 6 – source data 1). We again used repetitive stimulation to probe for cell-specific plasticity in MC responsiveness. In unlabeled MCs, firing was stable across trials, or even increased slightly over time (Figures 6E-F; spike count of 10th vs. 1st trial, $115 \pm 17\%$,

peak firing rate, $87.0 \pm 11.4\%$). In contrast, the output of GFP(+) MCs decreased markedly over successive stimuli (Figures 6F-H; spike count of 10th vs. 1st trial, $30.7 \pm 12.3\%$; peak firing, $29.4 \pm 10.2\%$). Results were independent of criteria for selecting GFP(+) and GFP(-) populations (Figure 6 – figure supplement 1). These data indicate that reduced excitability arises specifically in the MC ensemble activated by the stud during mating and subsequent sensory experience.

To ensure that MC excitability was altered by learning, rather than reflecting a pre-existing cell population in AOB, we performed parallel experiments where control females received sensory exposure to males without mating. This labeled a much smaller group of MCs, which responded with higher firing rates than unlabeled neurons in the same animals (Figure 6 – figure supplement 2A-C). Membrane resistance was also higher in GFP(+) MCs (data not shown), suggesting that sensory stimulation alone preferentially recruits a group of high-excitability neurons similar to findings in neocortex (Yassin et al., 2010). In contrast to results in mated females, however, both GFP(-) and GFP(+) populations maintained consistent firing over all trials, despite their differences in initial responsiveness (Figure 6 – figure supplement 1D-F). These data further indicate that dynamic changes in MC excitability result from imprinting, and emerge specifically in the population labeled during mating.

We estimated the net loss of output for stud-activated MC populations by plotting cumulative spike counts for matched groups of GFP(+) and GFP(-) neurons, which showed that total spike count diverged rapidly between the two groups (Figure 6I). Together, these results provide the first direct evidence of targeted, cell-specific changes in the AOB ensembles activated by conspecifics during social experience.

MC firing could potentially be shaped directly by changes in intrinsic membrane properties *per se*, or by prolonged synaptic inhibition that outlasts the stimulus. To distinguish between these possibilities, we tested MCs after blocking fast synaptic transmission with NBQX, APV, and bicuculline (10, 50, and 10 μ M respectively). MC suppression was intact even after eliminating local circuit interactions, indicating that it did not depend on persistent inhibition (Figure 7- figure supplement 1). We further probed the source of reduced MC firing by examining membrane properties over the course of stimulus trains. Repeated stimulation led to a progressive hyperpolarization of MC membrane potential, both in randomly selected MCs in mated Arc-GFP females (Fig. 7A) and in GFP(+) MCs in mated Fos-GFP mice (Figure 7B; Figure 7 – source data 1). These changes were not predicted by initial MC resting potential, which was indistinguishable between naïve and mated females in Arc-GFP mice (Figure 7C; -58.0 ± 1.1 mV vs. -56.7 ± 0.7 mV respectively), and between GFP(+) and GFP(-) populations within mated Fos-GFP females (Figure 7C; -55.0 ± 1.5 vs. -53.9 ± 1.1 mV, $p = 0.56$, t-test; $n = 7$ and 11 respectively). On average, GFP(+) MCs were hyperpolarized by -3.3 ± 0.5 mV vs. 0.2 ± 0.6 for GFP(-) neurons (Figure 7D; $p < 0.05$, t-test). MC hyperpolarization was strongly correlated with loss of firing (Figure 7E). Hyperpolarization was accompanied by a slight reduction in membrane resistance (initial vs. final R_{in} , 486 ± 114 M Ω vs. 341 ± 27 M Ω ; $p = 0.26$, t-test). Together, these data further indicate that reduced MC output is due to changes in intrinsic membrane properties rather than altered synaptic inhibition, imparting stimulus-activated neurons with a sensitivity to recent firing that progressively dampens their output.

The hormonal changes that drive pregnancy block occur over several hours of sensory exposure, during which animals interact intermittently at varying intervals. To further probe the time course of plasticity, we probed randomly selected MCs in mated females using stimuli spaced 2 min and 3 min apart. Each firing bout led to hyperpolarization that decayed extremely slowly, lasting until the onset of the next stimulus (Figure 7G). Intervals of both 2 min and 3 min gave comparable levels of hyperpolarization and attenuated firing after 10 stimuli (Figures 7G-H; mean ΔV_m , -5.64 ± 0.88 and -6.02 ± 2.05 mV for 2 and 3 min intervals respectively; normalized spike count, 0.176 ± 0.116 and 0.193 ± 0.089 for 2 and 3 min). When possible, we tested MCs again at 15 min and 35 min after the offset of stimulation, which revealed that suppression lasted for total periods of an hour or longer (normalized spike count, 0.149 ± 0.080 and 0.117 ± 0.072 at 15 and 35 min respectively; ΔV_m , -5.85 ± 1.49 and -6.21 ± 1.97 at 15 and 35 min). These results indicate that MC plasticity persists on the timescales relevant to physiology and behavior in vivo.

Discussion

Our data provide the first direct measurements of the synaptic and cellular effects of pheromonal learning in females after mating. We used *ex vivo* recordings to characterize changes in both excitatory and inhibitory neurons in AOB, and found broad enhancement of inhibitory circuits consistent with previous findings. However, using targeted measurements from identified mating-activated ensembles, we found that synaptic plasticity lacked the specificity thought to be required for recognition memories.

Surprisingly, we also found a striking reduction in intrinsic excitability in MCs, suggesting a novel basis for storing sensory experience in AOB. Notably, this loss of responsiveness was confined to the set of MCs activated during mating, consistent with a stud-selective recognition memory. MC excitability also showed unusual dynamics, where output was initially unchanged, but instead progressively decreased depending on recent activity. Slow MC dynamics may selectively filter repetitive vomeronasal inputs over extended timescales, preserving sensitivity at the onset of behavioral encounters while reducing their longer-term impact on neuroendocrine centers that control hormonal status and pregnancy. Our data are broadly consistent with the selective MC plasticity proposed by existing learning models, but also suggest a new and unanticipated cellular mechanism that complements changes in synaptic strength.

Inhibitory circuits in AOB

AOB inhibitory circuits had several unique properties. First, we found that MCs could robustly suppress their own firing via pronounced self-inhibition, consistent with robust GABAergic circuits in AOB (Castro et al., 2007; Hendrickson et al., 2008; Shpak et al., 2012). Self-inhibition in MOB MCs, in contrast, had much weaker effects on firing. Self-inhibition in AOB also emerged surprisingly slowly, building over several seconds so that it was strongest during prolonged MC firing on the timescales of natural sensory-evoked responses (Ben-Shaul et al., 2010; Luo et al., 2003). The basis for differences in self-inhibition in AOB and MOB are unclear, but may be linked to the prominent role of mGluRs in AOB (Castro et al., 2007).

Our data suggest that mating acts on multiple cell types and synaptic elements in AOB inhibitory circuits. Increased frequency of excitatory input to GCs implies upregulation of release sites in MC dendrites, and enhanced amplitude suggests strengthening of postsynaptic contacts, consistent with the ultrastructural enlargements seen in the postsynaptic density (Ichikawa, 2003; Matsuoka et al., 2004). Increased frequency of mIPSCs in MCs also suggests enhanced release of GABA from GCs, which could result either from changes in existing contacts or addition of new synapses via spine growth or recruitment of adult-born interneurons (Mak and Weiss, 2010; Shingo et al., 2003). Overall, however, this inhibitory plasticity appeared to have little effect on MC output driven by current injection. Increased release of GABA may be counterbalanced by short-term dynamics during extended firing (Dietz and Murthy, 2005), or alternatively changes in mIPSCs may reflect top-down inputs to AOB (Fan and Luo, 2009) that would contribute to spontaneous but not recurrent inhibition.

Memory formation has long been proposed to rely on inhibitory plasticity, selectively targeting the stud-activated MC population (Brennan and Keverne, 1997). In contrast, we found that synaptic changes were widely distributed across both MCs and GCs with no observable dependence on activation during mating. While non-specific plasticity runs counter to existing models, our data do not exclude a role for inhibition in learning or sensory processing. GABAergic circuits may be differentially recruited *in vivo*, where complex natural cues activate larger MC populations (Ben-Shaul et al., 2010; Meeks et al., 2010). Inhibition strongly shapes MC firing in the intact brain (Hendrickson et al., 2008), and descending pathways targeting AOB are likely to further shape sensory responses (Fan and Luo, 2009). Overall, however, the nonspecific nature of

inhibitory plasticity suggests it may act in concert with other, more targeted changes in the AOB circuit.

Plasticity of intrinsic membrane excitability in MCs

Unexpectedly, imprinting had the most striking effects on intrinsic rather than synaptic properties, suggesting an alternative cellular mechanism for storing sensory experience in AOB. MC suppression was largely absent in naïve females, but was strongly increased by mating in two separate datasets, indicating that it is was generated *de novo* by learning rather than reflecting pre-existing AOB populations (Yassin et al., 2010). Experience-dependent changes in excitability often accompany synaptic modifications in both mammalian and invertebrate systems (Daoudal and Debanne, 2003; Zhang and Linden, 2003). Altered intrinsic properties support homeostatic regulation in cortical circuits, scaling cellular excitability to match long-term changes in sensory input (Desai et al., 1999; Turrigiano, 2011). Often, learning acts to enhance excitability (Barkai and Saar, 2001; Zhang and Linden, 2003), acting to amplify responses to trained sensory inputs (Mozzachiodi and Byrne, 2010), or to select neural populations encoding the learned cue (Yiu et al., 2014; Zhou et al., 2009). Here, in contrast, MC excitability was strongly reduced by pheromonal learning. This sign reversal is consistent with the fact that imprinting leads to the suppression of an otherwise default neuroendocrine response to sensory input. Notably, whereas other paradigms lead to static effects on excitability that are immediately apparent on testing, changes in MCs were dynamic and only emerged after strong activation. The

excitability of control and ‘imprinted’ neurons was initially indistinguishable, and responses only diverged after cells had experienced substantial firing. MC hyperpolarization accumulated after each trial and lasted for at least 30 min after the offset of stimulation, suggesting that MCs display an unusual and highly integrative form of intrinsic membrane plasticity.

What are the potential advantages of intrinsic versus synaptic plasticity in AOB? Membrane excitability offers a simple way to selectively control the output of specific MC populations, whereas inhibitory plasticity would need to be coordinated across large sets of GCs, and further targeted to the specific synapses onto stud-encoding MCs. Intrinsic excitability may be particularly well suited to mediating learning in dedicated sensory pathways coupled to stereotyped behavioral responses. Interestingly, firing was similar for labeled and unlabeled MCs after mating, and only diverged after extended activity bouts. Thus, learning does not cause simple, static changes in MC excitability *per se*, but instead leads to metaplastic effects that impart sensitivity to recent firing levels. In metaplasticity of synaptic strength, experience shifts thresholds for potentiation and depression via changes in NMDA subunit composition (Abraham, 2008; Lee et al., 2010). Metaplasticity in the intrinsic excitability of MCs may rely on similar changes in composition of membrane conductances. Prolonged hyperpolarization and lowered membrane resistance are consistent with changes in potassium channels such as HCN or Ca^{2+} -dependent K^{+} currents, which are present in main olfactory bulb and linked to learning in other systems (Lin et al., 2008; Nolan et al., 2004; Nolan et al., 2003; Stackman et al., 2002; Wang et al., 2007). MC firing is also modulated by intrinsic conductances such as CAN currents, which boost synaptic responses (Shpak et al.,

2014; Shpak et al., 2012) and likely contributed to accelerated firing rates seen over the first few seconds of stimulation in our study. Interestingly, this current opposes the MC hyperpolarization we describe here, which appeared to dominate after more prolonged firing bouts and was most readily apparent only after mating. AOB MCs thus appear to express multiple activity-dependent conductances that dynamically modulate their firing depending on the strength, duration, and biological context of activity. The specific conductances responsible for slow MC attenuation remain to be established.

Dynamic MC output and sensory representations

Dynamic, activity-dependent changes in excitability were a unique feature of AOB MCs. How may slowly adapting sensitivity contribute to sensory processing? One potential role is to high-pass filter vomeronasal input, preserving responsiveness at the onset of social interactions for appropriate selection of aggressive, reproductive, or parental behaviors (Burns-Cusato et al., 2004; Clancy et al., 1984; Stowers et al., 2002a; Tachikawa et al., 2013), while selectively attenuating the long-lasting, repetitive AOB activity required for the neuroendocrine changes that block pregnancy (Li et al., 1994; Rosser et al., 1989). Similarly, slow activity dynamics may help reduce interference between memories of different individuals. Different males have similar chemical signatures (Harvey et al., 1989), suggesting that they may also have overlapping neural representations in AOB. Eliminating the responses of stud-encoding MCs could therefore also disrupt representations of other, non-imprinted animals. Delayed changes in MC output may help minimize the impact of plasticity on overlapping sensory codes.

Fos-GFP labeling was transient, limiting our measurements to a period of several hours following mating. The effects of mating on pregnancy block, however, can last for many weeks (Brennan et al., 1990). It will be important to determine whether effects on MC excitability are maintained for similar time periods. Other, more permanent labeling strategies may allow plasticity to be tested at later time points (Guenthner et al., 2013; Sakurai et al., 2016). Alternatively, sensory memories could be stored initially in AOB and then transferred to other areas, as seen in other memory systems (Preston and Eichenbaum, 2013; Ross and Eichenbaum, 2006).

Mating is one of several biological contexts where animals show flexibility in vomeronasal-guided behaviors. Interestingly, many of these involve the loss of an otherwise default response, similar to the effects of mating. Males shift from attack to parental behaviors towards pups (Tachikawa et al., 2013; Wu et al., 2014), and regulate aggression towards other males to form dominance hierarchies (Wang et al., 2014). Behavioral responses to fear-inducing cues such as predator odors can also habituate with repeated presentation (Takahashi et al., 2005). It is currently unclear whether the behavioral plasticity seen in other paradigms relies on similar cellular mechanisms in AOB, and it will be important for future work to test this possibility.

Overall, our data reveal a novel form of cellular plasticity that emerges after mating in females, where slowly emerging, activity-dependent changes in intrinsic excitability dramatically attenuate the output of the MC ensemble activated by the stud male. It will be important for future work to test how this plasticity shapes sensory representations and neuroendocrine responses in behaving animals during social encounters. Changes in MC excitability could also contribute to flexibility in other

vomeronasal-mediated behaviors, which often involve suppression of otherwise default sensory responses (Tachikawa et al., 2013). While the AOB is a critical node in the vomeronasal pathway, MC plasticity likely acts in parallel with broader changes across the extended network of brain regions that couple chemosensory input to behavior (Dulac et al., 2014; Wu et al., 2014).

Materials and methods

Mice

All experiments were performed in sexually mature adult female mice 8-14 weeks of age. Reporter lines were obtained from Jackson Laboratory (Arc-GFP, RRID:IMSR_JAX:007662; Fos-GFP, RRID:IMSR_JAX:018306) and bred in a C57Bl/6J background. Experimental Arc-GFP animals were heterozygous, maintaining a functional Arc allele. Animals were group housed in the Boston University animal care facility on a 12-h light/dark cycle with *ad lib* access to food and water. Mice were anesthetized ≥ 5 days prior to experiment and received bilateral ovariectomies followed by implantation of estradiol capsules (Bakker et al., 2003). On the experimental day, estrus was induced with progesterone injection (16 $\mu\text{g/g}$), confirmed by vaginal smears and histological examination (Caliqioni, 2009). At estrus onset, 3-4 hrs after the beginning of the light cycle, females were paired with a sexually experienced male in their home cage for an additional 4 hours for mating and subsequent sensory exposure required for imprinting. Males typically attempted copulation within 20-30 minutes.

Cases where males did not mount females were used as controls for sensory experience without mating. Sedated males were also used for sensory-exposure controls; activity-dependent labeling in the corresponding females was indistinguishable and these data were grouped together. Females in both mated and sensory-exposed groups were ovariectomized and progesterone-primed, while naïve females were unmanipulated. While mating success could not be evaluated in electrophysiology experiments, in a parallel group this protocol resulted in pregnancy in 9 of 11 gonadally intact females. Reproductive encounters were video recorded and scored to quantify mating and behavioral interactions. All procedures were approved by the Boston University Institutional Animal Care and Use Committee and followed guidelines set by the US National Institutes of Health.

Activity-dependent labeling

Activity-dependent labeling was visualized in each slice prior to electrophysiological recordings using a two-photon microscope (Prairie Ultima) with 920 nm excitation and a 20X NA 0.95 objective (Olympus), using consistent acquisition settings for laser power and detector gain across sessions. Immediately prior to establishing recordings, we acquired additional image stacks of GFP labeling for the field of view at each recording location (250 μ m X 250 μ m) using a 40X NA 0.8 objective (Olympus). Intensity was quantified for all detectable neurons using a circular region of interest centered on the soma. GFP intensity was continuously distributed, presumably reflecting graded levels of prior activity. Cells were classified as unlabeled or labeled using a threshold of ≤ 2 or ≥ 4 times background neuropil fluorescence respectively. For electrophysiological analysis, we performed similar analyses comparing the brightest third and dimmest 50%,

33%, and 25% of our recorded sample. Results were robust to classification threshold and comparison groups.

Electrophysiology

Sagittal brain slices of AOB (300 μ m thick) were prepared from female mice using a vibratome (VT1200S, Leica, Buffalo Grove IL). To preserve tissue health in adult animals, mice were deeply anesthetized with ketamine/xylazine and perfused transcardially with ice-cold modified artificial cerebrospinal fluid (ACSF) containing, in mM: 124 NaCl, 2.5 KCl, 1.25 NaH₂PO₄, 25 NaHCO₃, 75 sucrose, 10 glucose, 1.3 ascorbic acid, 0.5 CaCl₂ and 7 MgCl₂. Slices were maintained using ACSF containing, in mM: 124 NaCl, 3 KCl, 1.25 NaH₂PO₄, 26 NaHCO₃, 20 sucrose, 2 CaCl₂ and 1.5 MgCl₂, continuously oxygenated with 95/5% O₂/CO₂. Slices were visualized with a two-photon microscope (Ultima, Prairie Technologies, Middleton WI) using a 40x water immersion objective and Dodt contrast imaging. Whole cell electrodes were pulled to tip resistances of 3-8 M Ω and contained the following internal solutions (in mM): current clamp, 135 K-gluconate, 2 MgCl₂, 10 HEPES, 0.4 EGTA, 2 MgATP, 0.5 Na₃GTP, 10 phosphocreatine disodium; voltage clamp, 115 CsCl, 25 TEA-Cl, 5 QX314-Cl, 0.2 EGTA, 4 MgATP, 0.3 Na₃GTP and 10 phosphocreatine disodium. Alexa 594 was added to the internal solution to confirm cell identity in targeted recordings. Membrane voltage was not corrected for liquid junction potential. Electrophysiological data was collected at 29.5 $^{\circ}$ C with a Multiclamp 700B amplifier (Molecular Devices, Sunnyvale, CA) and digitized at 10 kHz (National Instruments PCI-6321) using custom Matlab routines (Mathworks, Natick, MA). Action potential detection and analysis was performed using custom Matlab routines detecting zero-crossing membrane potentials. Changes in firing with

repeated stimulation were quantified as a suppression index, calculated as the ratio of firing on the 10th vs. first trial. Synaptic currents and EPSPs were detected and analyzed in Igor Pro (WaveMetrics, Lake Oswego, Oregon) using Taro Tools (<https://sites.google.com/site/tarotoolsmember/>). Thresholds were chosen to maximize detection of synaptic events while excluding false positives due to recording noise. Thresholds were set at 10pA for mIPSCs in MCs, and 0.25 mV for EPSPs in GCs. In both cases we estimate we detected at least 95-98% of events while limiting false positives to <1%, determined by visual inspection. GC results were consistent across a wide range of detection criteria. All chemicals were obtained from Sigma/Aldrich (NBQX), Tocris (BMI), and Alomone Labs (TTX). Receptor antagonists (APV, NBQX and Gabazine) were applied by bath perfusion. All results reported in the text and figures represent mean \pm S.E.M.

Statistical analysis

Statistical significance was calculated using t-test or ANOVA as appropriate, noted in results and figure legends. Distributions of miniature and spontaneous synaptic events were analyzed with the Kolmogorov-Smirnov test. Animals were randomly assigned to naïve, sensory exposure, or mating groups after recovery from surgery. Data collection and analysis were not blind to experimental conditions.

References

- Abraham, N.M., Egger, V., Shimshek, D.R., Renden, R., Fukunaga, I., Sprengel, R., Seeburg, P.H., Klugmann, M., Margrie, T.W., Schaefer, A.T., and Kuner, T. 2010. Synaptic inhibition in the olfactory bulb accelerates odor discrimination in mice. *Neuron* 65, 399-411. doi: 10.1016/j.neuron.2010.01.009
- Abraham, W.C. 2008. Metaplasticity: tuning synapses and networks for plasticity. *Nat Rev Neurosci* 9, 387. doi: 10.1038/nrn2356
- Arnson, H.A., and Holy, T.E. 2013. Robust encoding of stimulus identity and concentration in the accessory olfactory system. *J Neurosci* 33, 13388-13397. doi: 10.1523/JNEUROSCI.0967-13.2013
- Bakker, J., Honda, S., Harada, N., and Balthazart, J. 2003. The aromatase knockout (ArKO) mouse provides new evidence that estrogens are required for the development of the female brain. *Annals of the New York Academy of Sciences* 1007, 251-262. doi:
- Barkai, E., and Saar, D. 2001. Cellular correlates of olfactory learning in the rat piriform cortex. *Reviews in the neurosciences* 12, 111-120. doi:
- Barth, A.L. 2007. Visualizing circuits and systems using transgenic reporters of neural activity. *Curr Opin Neurobiol* 17, 567-571. doi: 10.1016/j.conb.2007.10.003
- Ben-Shaul, Y., Katz, L.C., Mooney, R., and Dulac, C. 2010. In vivo vomeronasal stimulation reveals sensory encoding of conspecific and allospecific cues by the mouse accessory olfactory bulb. *Proc Natl Acad Sci U S A* 107, 5172-5177. doi: 10.1073/pnas.0915147107
- Brennan, P.A. 2004. The nose knows who's who: chemosensory individuality and mate recognition in mice. *Horm Behav* 46, 231-140. doi:
- Brennan, P.A., and Binns, E.K. 2005. Vomeronasal mechanisms of mate recognition in mice. *Chem Senses Suppl* 1, i148-149. doi:
- Brennan, P.A., Hancock, D., and Keverne, E.B. 1992. The expression of the immediate-early genes c-fos, egr-1 and c-jun in the accessory olfactory bulb during the formation of an olfactory memory in mice. *Neuroscience* 49, 277-284. doi:
- Brennan, P.A., Kaba, H., and Keverne, E.B. 1990. Olfactory recognition: a simple memory system. *Science* 250, 1223-1226. doi:
- Brennan, P.A., Kendrick, K.M., and Keverne, E.B. 1995. Neurotransmitter release in the accessory olfactory bulb during and after the formation of an olfactory memory in mice. *Neuroscience* 69, 1075-1086. doi:
- Brennan, P.A., and Keverne, E.B. 1997. Neural mechanisms of mammalian olfactory learning. *Prog Neurobiol* 51, 457-481. doi:

629 Bruce, H.M., and Parrott, D.M. 1960. Role of olfactory sense in pregnancy block by
630 strange males. *Science* 131, 1526. doi:

631 Burns-Cusato, M., Scordalakes, E.M., and Rissman, E.F. 2004. Of mice and missing
632 data: what we know (and need to learn) about male sexual behavior. *Physiol Behav* 83,
633 217-232. doi: 10.1016/j.physbeh.2004.08.015

634 Caliqioni, C.S. 2009. Assessing reproductive status/stages in mice. *Curr Protoc*
635 *Neurosci.* doi: 10.1002/0471142301.nsa04is48

636 Castro, J.B., Hovis, K.R., and Urban, N.N. 2007. Recurrent dendrodendritic inhibition of
637 accessory olfactory bulb mitral cells requires activation of group I metabotropic
638 glutamate receptors. *J Neurosci* 27, 5664-5671. doi: 10.1523/JNEUROSCI.0613-
639 07.2007

640 Chamero, P., Marton, T.F., Logan, D.W., Flanagan, K., Cruz, J.R., Saghatelian, A.,
641 Cravatt, B.F., and Stowers, L. 2007. Identification of protein pheromones that promote
642 aggressive behaviour. *Nature* 450, 899-902. doi: 10.1038/nature05997

643 Clancy, A.N., Coquelin, A., Macrides, F., Gorski, R.A., and Noble, E.P. 1984. Sexual
644 behavior and aggression in male mice: involvement of the vomeronasal system. *J*
645 *Neurosci* 4, 2222-2229. doi:

646 Daoudal, G., and Debanne, D. 2003. Long-term plasticity of intrinsic excitability: learning
647 rules and mechanisms. *Learning & memory* 10, 456-465. doi: 10.1101/lm.64103

648 Desai, N.S., Rutherford, L.C., and Turrigiano, G.G. 1999. Plasticity in the intrinsic
649 excitability of cortical pyramidal neurons. *Nat Neurosci* 2, 515-520. doi: 10.1038/9165

650 Dietz, S.B., and Murthy, V.N. 2005. Contrasting short-term plasticity at two sides of the
651 mitral-granule reciprocal synapse in the mammalian olfactory bulb. *The Journal of*
652 *physiology* 569, 475-488. doi: 10.1113/jphysiol.2005.095844

653 Dulac, C., O'Connell, L.A., and Wu, Z. 2014. Neural control of maternal and paternal
654 behaviors. *Science* 345, 765-770. doi: 10.1126/science.1253291

655 Dulac, C., and Torello, A.T. 2003. Molecular detection of pheromone signals in
656 mammals: from genes to behaviour. *Nat Rev Neurosci* 4, 551-562. doi:
657 10.1038/nrn1140

658 Fan, S., and Luo, M. 2009. The organization of feedback projections in a pathway
659 important for processing pheromonal signals. *Neuroscience* 161, 489-500. doi:
660 10.1016/j.neuroscience.2009.03.065

661 Guenther, C.J., Miyamichi, K., Yang, H.H., Heller, H.C., and Luo, L. 2013. Permanent
662 genetic access to transiently active neurons via TRAP: targeted recombination in active
663 populations. *Neuron* 78, 773-784. doi: 10.1016/j.neuron.2013.03.025

664 Halem, H.A., Cherry, J.A., and Baum, M.J. 2001. Central forebrain Fos responses to
 665 familiar male odours are attenuated in recently mated female mice. *Eur J Neurosci* 13,
 666 389-399. doi:

667 Harvey, S., Jemiolo, B., and Novotny, M. 1989. Pattern of volatile compounds in
 668 dominant and subordinate male mouse urine. *J Chem Ecol* 15, 2061-2072. doi:
 669 10.1007/BF01207438

670 Hendrickson, R.C., Krauthamer, S., Essenberg, J.M., and Holy, T.E. 2008. Inhibition
 671 shapes sex selectivity in the mouse accessory olfactory bulb. *J Neurosci* 28, 12523-
 672 12534. doi: 10.1523/JNEUROSCI.2715-08.2008

673 Hull, E.M., and Dominguez, J.M. 2007. Sexual behavior in male rodents. *Horm Behav*
 674 52, 45-55. doi:

675 Hurst, J.L. 2009. Female recognition and assessment of males through scent. *Behav*
 676 *Brain Res* 200, 295-303. doi: 10.1016/j.bbr.2008.12.020

677 Ichikawa, M. 2003. Synaptic mechanisms underlying pheromonal memory in
 678 vomeronasal system. *Zoolog Sci* 20, 687-695. doi:

679 Isaacson, J.S., and Strowbridge, B.W. 1998. Olfactory reciprocal synapses: dendritic
 680 signaling in the CNS. *Neuron* 20, 749-761. doi:

681 Kaba, H., Hayashi, Y., Higuchi, T., and Nakanishi, S. 1994. Induction of an olfactory
 682 memory by the activation of a metabotropic glutamate receptor. *Science* 265, 262-264.
 683 doi:

684 Kaba, H., and Keverne, E.B. 1988. The effect of microinfusions of drugs into the
 685 accessory olfactory bulb on the olfactory block to pregnancy. *Neuroscience* 25, 1007-
 686 1011. doi:

687 Kendrick, K.M., Levy, F., and Keverne, E.B. 1992. Changes in the sensory processing
 688 of olfactory signals induced by birth in sheep. *Science* 256, 833-836. doi:

689 Keverne, E.B., and Brennan, P.A. 1996. Olfactory recognition memory. *Journal of*
 690 *physiology, Paris* 90, 399-401. doi:

691 Kimchi, T., Xu, J., and Dulac, C. 2007. A functional circuit underlying male sexual
 692 behaviour in the female mouse brain. *Nature* 448, 1009-1014. doi: 10.1038/nature06089

693 Lee, M.C., Yasuda, R., and Ehlers, M.D. 2010. Metaplasticity at single glutamatergic
 694 synapses. *Neuron* 66, 859-870. doi: 10.1016/j.neuron.2010.05.015

695 Levy, F., Keller, M., and Poindron, P. 2004. Olfactory regulation of maternal behavior in
 696 mammals. *Hormones and Behavior* 46, 284-302. doi:

697 Li, C.S., Kaba, H., and Seto, K. 1994. Effective induction of pregnancy block by
698 electrical stimulation of the mouse accessory olfactory bulb coincident with prolactin
699 surges. *Neurosci Lett* 176, 5-8. doi:

700 Lin, M.T., Lujan, R., Watanabe, M., Adelman, J.P., and Maylie, J. 2008. SK2 channel
701 plasticity contributes to LTP at Schaffer collateral-CA1 synapses. *Nat Neurosci* 11, 170-
702 177. doi:

703 Luo, M., Fee, M.S., and Katz, L.C. 2003. Encoding pheromonal signals in the accessory
704 olfactory bulb of behaving mice. *Science* 299, 1196-1201. doi:
705 10.1126/science.1082133

706 Mak, G.K., and Weiss, S. 2010. Paternal recognition of adult offspring mediated by
707 newly generated CNS neurons. *Nat Neurosci* 13, 753-758. doi: 10.1038/nn.2550

708 Margrie, T.W., Sakmann, B., and Urban, N.N. 2001. Action potential propagation in
709 mitral cell lateral dendrites is decremental and controls recurrent and lateral inhibition in
710 the mammalian olfactory bulb. *Proc Natl Acad Sci USA* 98, 319-324. doi:

711 Matsuoka, M., Kaba, H., Mori, Y., and Ichikawa, M. 1997. Synaptic plasticity in olfactory
712 memory formation in female mice. *Neuroreport* 8, 2501-2504. doi:

713 Matsuoka, M., Kaba, H., Moriya, K., Yoshida-Matsuoka, J., Costanzo, R.M., Norita, M.,
714 and Ichikawa, M. 2004. Remodeling of reciprocal synapses associated with persistence
715 of long-term memory. *Eur J Neurosci* 19, 1668-1672. doi: 10.1111/j.1460-
716 9568.2004.03271.x

717 Matsuoka, M., Yoshida-Matsuoka, J., Sugiura, H., Yamagata, K., Ichikawa, M., and
718 Norita, M. 2002. Mating behavior induces differential Arc expression in the main and
719 accessory olfactory bulbs of adult rats. *Neurosci Lett* 335, 111-114. doi:

720 Meeks, J.P., Arnson, H.A., and Holy, T.E. 2010. Representation and transformation of
721 sensory information in the mouse accessory olfactory system. *Nat Neurosci* 13, 723-730.
722 doi: 10.1038/nn.2546

723 Mozzachiodi, R., and Byrne, J.H. 2010. More than synaptic plasticity: Role of
724 nonsynaptic plasticity in learning and memory. *Trends Neurosci* 33, 17-35. doi:

725 Nolan, M.F., Malleret, G., Dudman, J.T., Buhl, D.L., Santoro, B., Gibbs, E., Vronskaya,
726 S., Buzsaki, G., Siegelbaum, S.A., Kandel, E.R., and Morozov, A. 2004. A behavioral
727 role for dendritic integration: HCN1 channels constrain spatial memory and plasticity at
728 inputs to distal dendrites of CA1 pyramidal neurons. *Cell* 119, 719-732. doi:

729 Nolan, M.F., Malleret, G., Lee, K.H., Gibbs, E., Dudman, J.T., Santoro, B., Yin, D.,
730 Thompson, R.F., Siegelbaum, S.A., Kandel, E.R., and Morozov, A. 2003. The
731 hyperpolarization-activated HCN1 channel is important for motor learning and neuronal
732 integration by cerebellar Purkinje cells. *Cell* 115, 551-564. doi:

733 Preston, A.R., and Eichenbaum, H. 2013. Interplay of hippocampus and prefrontal
734 cortex in memory. *Current biology : CB* 23, R764-773. doi: 10.1016/j.cub.2013.05.041

735 Reijmers, L., and Mayford, M. 2009. Genetic control of active neural circuits. *Front Mol*
736 *Neurosci* 2. doi: 10.3389/neuro.02.027.2009

737 Reijmers, L.G., Perkins, B.L., Matsuo, N., and Mayford, M. 2007. Localization of a
738 stable neural correlate of associative memory. *Science* 317, 1230-1233. doi:
739 10.1126/science.1143839

740 Ross, R.S., and Eichenbaum, H. 2006. Dynamics of hippocampal and cortical activation
741 during consolidation of a nonspatial memory. *J Neurosci* 26, 4852-4859. doi:
742 10.1523/JNEUROSCI.0659-06.2006

743 Rosser, A.E., Remfry, C.J., and Keverne, E.B. 1989. Restricted exposure of mice to
744 primer pheromones coincident with prolactin surges blocks pregnancy by changing
745 hypothalamic dopamine release. *J Reprod Fertil* 87, 553-559. doi:

746 Sakurai, K., Zhao, S., Takatoh, J., Rodriguez, E., Lu, J., Leavitt, A.D., Fu, M., Han, B.X.,
747 and Wang, F. 2016. Capturing and Manipulating Activated Neuronal Ensembles with
748 CANE Delineates a Hypothalamic Social-Fear Circuit. *Neuron* 92, 739-753. doi:
749 10.1016/j.neuron.2016.10.015

750 Shepherd, G.M., and Greer, C.A. (1998). Olfactory Bulb. In *The Synaptic Organization*
751 *of the Brain*, G.M. Shepherd, ed. (New York: Oxford University Press), pp. 159-204.

752 Shingo, T., Gregg, C., Enwere, E., Fujikawa, H., Hassam, R., Geary, C., Cross, J.C.,
753 and Weiss, S. 2003. Pregnancy-stimulated neurogenesis in the adult female forebrain
754 mediated by prolactin. *Science* 299, 117-120. doi: 10.1126/science.1076647

755 Shpak, G., Zylbertal, A., and Wagner, S. 2014. Transient and sustained
756 afterdepolarizations in accessory olfactory bulb mitral cells are mediated by distinct
757 mechanisms that are differentially regulated by neuromodulators. *Front Cell Neurosci* 8,
758 432. doi: 10.3389/fncel.2014.00432

759 Shpak, G., Zylbertal, A., Yarom, Y., and Wagner, S. 2012. Calcium-activated sustained
760 firing responses distinguish accessory from main olfactory bulb mitral cells. *J Neurosci*
761 32, 6251-6262. doi:

762 Stackman, R.W., Hammond, R.S., Linardatos, E., Gerlach, A., Maylie, J., Adelman, J.P.,
763 and Tzounopoulos, T. 2002. Small conductance Ca²⁺-activated K⁺ channels modulate
764 synaptic plasticity and memory encoding. *J Neurosci* 22, 10163-10171. doi:

765 Stowers, L., Holy, T., Meister, M., Dulac, C., and Koentges, G. 2002a. Loss of sex
766 discrimination and male-male aggression in mice deficient for TRP2. *Science* 295,
767 1493-1500. doi:

768 Stowers, L., Holy, T.E., Meister, M., Dulac, C., and Koentges, G. 2002b. Loss of sex
 769 discrimination and male-male aggression in mice deficient for TRP2. *Science* 295,
 770 1493-1500. doi: 10.1126/science.1069259

771 Strom, J.O., Theodorsson, A., Ingberg, E., Isaksson, I.M., and Theodorsson, E. 2012.
 772 Ovariectomy and 17beta-estradiol replacement in rats and mice: a visual demonstration.
 773 *J Vis Exp*, e4013. doi: 10.3791/4013

774 Tachikawa, K.S., Yoshihara, Y., and Kuroda, K.O. 2013. Behavioral transition from
 775 attack to parenting in male mice: a crucial role of the vomeronasal system. *J Neurosci*
 776 33, 5120-5126. doi:

777 Takahashi, L.K., Nakashima, B.R., Hong, H., and Watanabe, K. 2005. The smell of
 778 danger: a behavioral and neural analysis of predator odor-induced fear. *Neurosci*
 779 *Biobehav Rev* 29, 1157-1167. doi: 10.1016/j.neubiorev.2005.04.008

780 Tirindelli, R., Dibattista, M., Pifferi, S., and Menini, A. 2009. From pheromones to
 781 behavior. *Physiol Rev* 89, 921-956. doi: 10.1152/physrev.00037.2008

782 Tolokh, I., Fu, X., and Holy, T. 2013. Reliable sex and strain discrimination in the mouse
 783 vomeronasal organ and accessory olfactory bulb. *J Neurosci* 33, 13903-13913. doi:

784 Turrigiano, G. 2011. Too many cooks? Intrinsic and synaptic homeostatic mechanisms
 785 in cortical circuit refinement. *Annu Rev Neurosci* 34, 89-103. doi: 10.1146/annurev-
 786 neuro-060909-153238

787 Wallace, D.L., Han, M.H., Graham, D.L., Green, T.A., Vialou, V., Iniguez, S.D., Cao, J.L.,
 788 Kirk, A., Chakravarty, S., Kumar, A., *et al.* 2009. CREB regulation of nucleus
 789 accumbens excitability mediates social isolation-induced behavioral deficits. *Nat*
 790 *Neurosci* 12, 200-209. doi: 10.1038/nn.2257

791 Wang, F., Kessels, H.W., and Hu, H. 2014. The mouse that roared: neural mechanisms
 792 of social hierarchy. *Trends Neurosci* 37, 674-682. doi: 10.1016/j.tins.2014.07.005

793 Wang, K.H., Majewska, A., Schummers, J., Farley, B., Hu, C., Sur, M., and Tonegawa,
 794 S. 2006. In vivo two-photon imaging reveals a role of arc in enhancing orientation
 795 specificity in visual cortex. *Cell* 126, 389-402. doi: 10.1016/j.cell.2006.06.038

796 Wang, M., Ramos, B.P., Paspalas, C.D., Shu, Y., Simen, A., Dugue, A., Vijayraghavan,
 797 S., Brennan, A., Dudley, A., Nou, E., *et al.* 2007. Alpha2A-adrenoceptors strengthen
 798 working memory networks by inhibiting cAMP-HCN channel signaling in prefrontal
 799 cortex. *Cell* 129, 397-410. doi:

800 Wu, Z., Autry, A.E., Bergan, J.F., Watabe-Uchida, M., and Dulac, C.G. 2014. Galanin
 801 neurons in the medial preoptic area govern parental behaviour. *Nature* 509, 325-330.
 802 doi: 10.1038/nature13307

803 Yassin, L., Benedetti, B.L., Jouhanneau, J.-S., Wen, J., Poulet, J.F.A., and Barth, A.L.
804 2010. An embedded subnetwork of highly active neurons in the neocortex. *Neuron* 68,
805 1043-1050. doi:

806 Yiu, A.P., Mercaldo, V., Yan, C., Richards, B., Rashid, A.J., Hsiang, H.L., Pressey, J.,
807 Mahadevan, V., Tran, M.M., Kushner, S.A., *et al.* 2014. Neurons are recruited to a
808 memory trace based on relative neuronal excitability immediately before training.
809 *Neuron* 83, 722-735. doi: 10.1016/j.neuron.2014.07.017

810 Young, L.J., and Wang, Z. 2004. The neurobiology of pair bonding. *Nat Neurosci* 7,
811 1048-1054. doi:

812 Zhang, W., and Linden, D.J. 2003. The other side of the engram: experience-driven
813 changes in neuronal intrinsic excitability. *Nat Rev Neurosci* 4, 885-900. doi:
814 10.1038/nrn1248

815 Zhou, Y., Won, J., Karlsson, M.G., Zhou, M., Rogerson, T., Balaji, J., Neve, R., Poirazi,
816 P., and Silva, A.J. 2009. CREB regulates excitability and the allocation of memory to
817 subsets of neurons in the amygdala. *Nat Neurosci* 12, 1438-1443. doi: 10.1038/nn.2405

818

Figures and Figure Legends

Figure 1. AOB MCs express robust, slowly emerging self-inhibition. (A)

Schematic of dendrodendritic self-inhibition pathway in MCs. **(B)** Left, dye-filled MC imaged after recording. S, soma; d, dendritic tufts that integrate sensory inputs; p, recording pipette. Right, brief, high-frequency spike trains trigger modest self-inhibition (gray, standard ACSF; black, after blocking inhibition with 15 μ M BMI; IPSP, inhibitory postsynaptic potential). **(C)** Pharmacologically isolated self-inhibition in AOB MCs. Colored traces show individual cells; black trace, average; mean $V_{inh} = -1.4 \pm 0.27$ mV ($n = 8$ cells in 5 mice). **(D,E)** Prolonged firing elicits robust MC self-inhibition in AOB but not MOB (black and purple respectively). Boxes show expanded view of barrages of IPSPs in AOB MCs, indicated by arrowheads, which only emerge after several seconds of firing. **(F)** Self-inhibition contributes to stronger decay of MC firing rates in AOB during extended stimuli ($n = 9$ and 9 cells in 5 and 5 mice for AOB and MOB respectively). **(G)** Initial and final firing rates during MC spike trains in MOB and AOB (purple and gray respectively).

Figure 1 – figure supplement 1. Robust self-inhibition regulates spiking of AOB

MCs. (A) Eliminating self-inhibition by blocking fast synaptic transmission increased the overall firing rate of MCs. **(B)** Blocking synaptic inhibition also eliminated the barrages of IPSPs that emerged later in train and persisted after the offset of spiking. **(C)** Firing of

841 AOB MCs is consistently enhanced after blocking inhibition ($p = 0.06$; t-test; $n = 6$ MCs
842 in 6 mice).

843

844

845 **Figure 2. Imprinting drives synaptic plasticity in both MCs and GCs. (A)**

846 Schematic of timeline for mating, sensory experience, and recording. **(B)** Inhibitory

847 synaptic inputs recorded in voltage-clamped MCs from naïve, sensory-exposed, and

848 mated mice. **(C,D)** Mating substantially increases mIPSC frequency. Left, cumulative

849 interval distributions; mated < naïve and exposed groups, $p = 0.002$ and 0.001

850 respectively. Right, mean frequency ($F=5.88$; $F_c = 3.20$; $p = 0.005$ for mated vs. naïve;

851 ANOVA with post-hoc Tukey test; $n = 18, 17$, and 15 cells in $5, 5$, and 6 mice

852 respectively). **(E,F)** The mean amplitude of mIPSCs was not significantly changed by

853 imprinting ($F=1.74$; $F_c = 3.20$; $p = 0.19$; ANOVA with post-hoc Tukey test), although

854 interval distributions were significantly smaller in the mated vs. naïve and sensory-

855 exposed groups ($p = 0.00007$ and 3×10^{-7} respectively). **(G)** Example traces showing

856 spontaneous EPSPs in GCs from naïve, sensory-exposed and mated mice. Rasters

857 indicate synaptic events. **(H,I)** Mating increased mean sEPSP frequency relative to both

858 naïve and sensory-exposed animals ($F = 6.64$; $F_c = 3.14$; $p = 0.00037$ and 0.038 for

859 mated vs. exposed and naïve mice respectively; ANOVA with post hoc Tukey test; $n =$

860 $17, 19$, and 30 cells in $5, 9$, and 12 mice). Interval distributions were significantly smaller

861 for mated vs. exposed and naïve animals ($p = 1 \times 10^{-11}$ and 0.0008 respectively). **(J,K)**

862 Mating also increased mean sEPSP amplitude in mated vs. naïve animals. Left,

863 cumulative distribution; right, mean amplitude ($F = 3.56$; $F_c = 3.14$; $p = 0.037$ for naïve

vs. mated, ANOVA with post hoc Tukey test). Amplitude distributions were larger for mated vs. naïve mice ($p = 0.04$). NS, not significant; *, $p < 0.05$; **, $p < 0.001$.

Figure 2 – figure supplement 1. Mating and sensory interactions during pairing.

(A) Video analysis of characteristic post-mating behavior between females and males.

Top, mating typically occurred early during the pairing period (red), followed by extensive and repetitive behavioral encounters including direct nasal contact required for vomeronasal activation (yellow). Bottom, expanded view of approximately 10 minutes of female-male interactions. (B) Distribution of intervals between investigatory bouts in the mated group (mean, 62.1 ± 7.99 sec; median, 15.9 sec; $n = 554$ bouts in 7 animals). (C) Investigatory behavior is elevated in mated relative to sensory-exposed groups (mean bouts per female, 89.5 ± 32.1 vs. 38 ± 11.6 respectively; $n = 7$ animals per group).

Figure 2 – figure supplement 2. Pharmacologically isolated inhibitory synaptic

currents in MCs. Top, inward currents recorded from voltage-clamped MCs using high-chloride pipette solution, measured in the presence of TTX, NBQX, and APV.

Bottom, miniature currents were completely blocked by addition of 15 μ M bicuculline.

Figure 2 – figure supplement 3. Synaptic effects in GCs are independent of event detection criteria. (A) Raw data traces with rasters showing synaptic events detected using thresholds of 0.25, 0.45, and 0.65 mV. (B) Mean frequency (left) and cumulative distribution of interevent interval (right) for excitatory synaptic input using a detection threshold of 0.45 mV. Mean frequency, 2.47 ± 0.53 , 2.43 ± 0.53 , and 4.69 ± 0.55 Hz; $F = 5.93$; $F_c = 3.14$; $p = 0.012$ and 0.038 for mated vs exposed and naïve groups respectively. (C) Mean and cumulative distribution of EPSP amplitudes for the same criteria. Mean amplitudes, 1.42 ± 0.08 , 1.62 ± 0.11 , and 1.85 ± 0.08 mV for naïve, exposed, and mated groups respectively. $F = 5.58$; $F_c = 3.14$; $p = 0.0047$ for mated vs. naïve groups. (D,E) Corresponding plots using a threshold of 0.65 mV. Mean frequency, 1.84 ± 0.51 , 1.80 ± 0.42 , and 3.38 ± 0.46 Hz; $F = 3.89$; $F_c = 3.14$; $p = 0.048$ for mated vs naïve groups. Mean amplitude, 1.70 ± 0.08 , 1.86 ± 0.11 , and 2.29 ± 0.09 mV for naïve, exposed, and mated groups respectively. $F = 10.52$; $F_c = 3.14$; $p = 0.0021$ and 0.0062 for mated vs. naïve and exposed groups respectively. *, $p < 0.05$; **, $p < 0.005$; all p values calculated using ANOVA with post-hoc Tukey test.

Figure 3. Synaptic plasticity is uncorrelated with activation during mating. (A) Arc-GFP labeling of AOB GCs activated by the stud male, visualized with live-tissue 2-photon imaging. Left, naïve control animal; right, mated female. Open arrowheads illustrate weakly labeled cells in control females; closed arrowheads, robust GC labeling after mating. (B) Fluorescence-targeted recordings of both unlabeled and labeled

populations of GCs. **(C,D)** Mean amplitude and frequency of sEPSPs are similar for GFP(-) and GFP(+) GCs in mated mice (amplitude: $p = 0.82$; frequency, $p = 0.58$; t-test; $n = 9$ and 13 cells in 10 mice, GFP(+) and (-) groups subdivided from data in Fig. 3 – figure supplement 1). **(E,F)** GFP labeling is uncorrelated with either amplitude or frequency of spontaneous excitatory input to GCs (regression slope not different from zero; amplitude: $p = 0.70$ and 0.22 for sensory-exposed and mated groups respectively; frequency: $p = 0.50$ and 0.92 ; linear regression t-test; $n = 17, 19$ and 30 neurons in 5, 9, and 12 mice for naïve, exposure and mated groups). **(G)** Fos-GFP labeling reveals a subpopulation of mating-activated MCs (arrowheads). **(H)** Targeted recordings of stimulated MCs. **(I,J)** Mean amplitude and frequency of mIPSCs are not significantly different between GFP(-) and GFP(+) MC populations ($p = 0.33$ and 0.38 respectively; t-test; $n = 8$ and 5 cells in 5 mice; groups subdivided from data in Fig. 2). **(K,L)** Amplitude and frequency of mIPSCs show no correlation with Fos-GFP intensity in MCs (regression slope not different from zero; $p = 0.64$ and 0.97 respectively; linear regression t-test; $n = 16$ neurons from 5 mice). Dashed lines show 95% confidence intervals.

Figure 3 – figure supplement 1. Mating increases fluorescent labeling in AOB and increases inhibitory synaptic input onto MCs. (A) Cumulative histogram of Arc-GFP intensity. Mating, but not sensory exposure alone, increases labeling in GCs ($p < 10^{-45}$, Kolmogorov–Smirnov test; $n = 14, 9$, and 18 slices for naïve, sensory-exposed, and mated groups respectively). **(B)** Mating produces robust increases in Fos-GFP labeling

of MCs ($p = 0.0004$, Kolmogorov–Smirnov test; $n = 8$ and 7 slices from 4 and 5 mice for naïve and mated groups respectively). **(C)** Representative synaptic currents measured from naïve and mated females. Currents are inward due to a high chloride recording solution. **(D)** Cumulative distribution of event amplitude ($p < 0.001$; Kolmogorov–Smirnov test; $n = 6$ and 16 cells in 3 and 5 mice). **(E)** The mean amplitude of inhibitory currents is unchanged in MCs from naïve and mated (red) animals ($p = 0.29$; t-test). **(F,G)** Mating increased the frequency of inhibitory input to MCs, reflected in both the leftward shift in the distribution of event intervals and increase in mean frequency ($p = 0.001$; t-test).

Figure 4. Experience alters intrinsic excitability of interneurons. (A)

Representative responses to graded current injection for GCs from naïve, sensory-exposed and mated mice. **(B)** Current-firing plot shows a shift towards increased excitability of GCs from both mated and sensory-exposed females. **(C)** GC resting membrane potential was significantly hyperpolarized after mating ($p = 0.008$ for mated vs. naïve; ANOVA with post-hoc Tukey test; $F = 5.18$; $F_c = 3.14$; $n = 17, 19$, and 31 cells from $5, 9$, and 12 mice for naïve, sensory-exposed, and mated groups respectively). **(D)** The slope of the current-firing function was similar across groups ($0.28 \pm 0.01, 0.27 \pm 0.02$, and 0.28 ± 0.01 ; $F = 0.14$; $F_c = 3.15$; $p = 0.87$; ANOVA with post-hoc Tukey test). **(E)** GC resting potential was uncorrelated with intensity of Arc-GFP labeling in both sensory-exposed and mated animals (slope not significantly different from zero; $p = 0.87, 0.37$ and 0.81 for naïve, sensory-exposed and mated

groups respectively; linear regression test; $n = 17, 19$ and 31 cells in $5, 9$ and 12 mice).

(F) In mated females, resting potential was indistinguishable between GFP(-) and

GFP(+) GCs (-66.8 ± 2.19 vs. -65.4 ± 1.85 mV respectively; $p = 0.62$, t-test; $n = 10$ and

13 cells in 10 mice, subdivided from the mated group in panel E). NS, not significant; *,

$p < 0.01$.

Figure 5. Mating reduces the responsiveness of MCs to repetitive inputs. (A) MC

firing to an initial current stimulus is similar for naïve and mated females. **(B)** Firing rate

profile averaged across all MCs from naïve and mated animals. **(C, D)** Mating has no

effect initial MC output (peak firing rate: $p = 0.51$; change in firing rate: $p = 0.55$; t-test; n

$= 10$ and 15 cells from 5 and 7 mice for naïve and mated groups respectively). **(E)**

Example MC responses to repetitive stimulation. Firing is stable over time in naïve

females, but drops dramatically over time after mating. **(F)** Average MC output across

successive stimuli for naïve (blue) and mated females (red). Firing on 10^{th} trial is $80 \pm$

11% (naïve) vs. $36 \pm 8\%$ of 1^{st} trial (mated); $F = 10.01$, $F_c = 4.30$, $p = 0.003$; ANOVA

with post-hoc Tukey test. Light colors show individual neurons; dark traces show mean

\pm SEM. **(G)** Cumulative histogram showing increased attenuation in MCs from mated

animals ($p = 0.027$; Kolmogorov-Smirnov test; $n = 9$ and 15 neurons from 5 and 7 mice

respectively). NS, not significant. *, $p < 0.05$; **, $p < 0.01$.

Figure 6. Plasticity in MC responsiveness is specific to mating-activated neurons.

(A) Both GFP(-) and GFP(+) MCs show similar initial responses to current stimuli. **(B)** Mean firing rate profiles for GFP(+) and GFP(-) MCs in Fos-GFP females after mating (mean \pm SEM; n = 7 and 11 cells in 5 and 7 mice). **(C, D)** Initial MC output is similar between GFP(-) and GFP(+) groups (firing rate, p = 0.81; spike count, p = 0.63; t-test). **(E)** Representative MC responses to repetitive stimulation in mated females. **(F)** After mating, GFP(-) MCs maintain consistent firing, but the output of stud-activated GFP(+) neurons is dramatically attenuated over time (mean \pm SEM; n = 7 and 11 cells in 7 mice). **(G)** Cumulative histograms indicate a shift towards greater suppression in the MCs activated during mating (p = 0.18; Kolmogorov-Smirnov test). **(H)** Mean suppression after 10 trials for GFP(-) and GFP(+) neurons (spike count on 10th vs. 1st trial: unlabeled, 115 \pm 17%, p = 0.41; labeled, 30.7 \pm 12.3%; p = 0.0017; t-test). **(I)** Cumulative action potential output of GFP(-) and GFP(+) MCs, averaged across all recorded neurons.

Figure 6 – figure supplement 1. Correlated plasticity and GFP labeling are

independent of selection criteria. **(A)** Arc-GFP labeling intensity for the GCs in our recording sample (green markers) superimposed on the distribution for all detectable GCs (gray line, normalized exponential fit to imaging data). Our dataset spans the majority of intensity values. **(B, C, D)** Frequency and amplitude of sEPSPs and resting membrane potential of GCs, respectively. Results comparing GFP(+) and GFP(-) populations are consistent across various selection criteria (upper vs. lower 1/2, 1/3,

999 and 1/4 of the recorded cells). **(E)** Fos-GFP labeling intensity for recorded MCs as in (A).
1000 Triangles indicate cells used to analyze synaptic inhibition; circles, cells used to analyze
1001 slow firing suppression. **(F, G, H)** mIPSC frequency, mIPSC amplitude, and firing rate
1002 suppression for repetitive stimuli, respectively. Results were again consistent across a
1003 range of selection criteria.
1004

Figure 6 – figure supplement 2. Slow attenuation is absent in GFP(+) MCs labeled by sensory exposure alone. (A) Firing rates are elevated in GFP(+) MCs relative to unlabeled neurons. **(B, C)** Increased firing rates for initial stimuli in GFP(+) vs. GFP(-) MCs in the absence of mating. Peak rates, 30.5 ± 2.2 Hz vs. 15.5 ± 2.7 Hz respectively, mean \pm SEM; $p < 0.05$, t-test; $n = 5$ and 7 cells in 4 mice). **(D)** Example MC responses to repetitive current injection for both GFP(-) and GFP(+) neurons. **(E)** In the absence of mating, both MC groups maintain stable output (mean \pm SEM; $n = 5$ and 7 cells in 4 mice). **(F)** GFP(+) and GFP(-) cells show similar levels of suppression on trial 10 ($p = 0.77$; t-test).

Figure 7. Loss of MC sensitivity results from progressive membrane potential hyperpolarization. (A) Representative MC responses to repetitive stimulation, showing initial resting potential and onset of firing for each trial. Progressive hyperpolarization was greatly enhanced in mated vs. naïve mice (red and blue respectively). **(B)** Within the AOB of mated females, hyperpolarization was selectively expressed in mating-activated GFP(+) MC populations. **(C)** Initial resting membrane potential was similar for MCs from naïve vs. mated females (blue and red respectively; $p = 0.76$; $n = 9$ and 15 cells in 5 and 7 mice), and for labeled and unlabeled MC populations in mated animals (gray and green; $p = 0.56$; t-test; $n = 7$ and 11 neurons in 5 and 7 mice). **(D)** Mean hyperpolarization during repetitive stimulation for GFP(+) and GFP(-) MCs (green and gray; upper and lower 1/3 of the recorded population; *, $p <$

0.05; t-test). **(E)** Progressive loss of MC responsiveness is correlated with membrane hyperpolarization. Green, GFP(+); dark gray, GFP(-); light gray, intermediate. **(F)** Membrane hyperpolarization persists for >2.5 minutes between stimuli. Traces show Vm before and after 3 successive spike trains delivered 3 mins apart. Red dashes show step-like hyperpolarization lasting until the next stimulus. **(G,H)** Mean hyperpolarization and normalized change in firing for MCs tested with stimuli 2 min and 3 min apart.

Figure 7 – figure supplement 1. MC hyperpolarization and attenuation of firing does not depend on persistent synaptic inhibition. (A) Representative MC membrane potential response after blocking fast synaptic transmission with NBQX, APV, and bicuculline (5, 50, and 10 μ M respectively). **(B)** Decreased MC output over the course of 10 stimuli correlates strongly with membrane hyperpolarization.

Figure 1 - source data 1.

This spreadsheet contains the initial and final firing rates for the individual neurons shown in Figure 1G. These data can be opened with Microsoft Excel or with open-source alternatives such as OpenOffice.

Figure 2 - source data 1.

This spreadsheet contains the mean frequency and amplitude data for the individual neurons used to generate the bar plots shown in Figures 2D and 2F (mitral cell mIPSCs) and 2I and 2K (granule cell mEPSCs). These data can be opened with Microsoft Excel or with open-source alternatives such as OpenOffice.

Figure 3 - source data 1.

This spreadsheet contains the mean frequency and amplitude data for the individual neurons used to generate the bar plots shown in Figures 3C, 3D, 3I, and 3J, comparing synaptic inputs to GFP(-) and GFP(+) neurons. These data can be opened with Microsoft Excel or with open-source alternatives such as OpenOffice.

Figure 4 - source data 1.

This spreadsheet contains the resting membrane potential and firing rate data for the individual neurons used to generate the bar plots shown in Figures 4C, 4D, and 4F.

These data can be opened with Microsoft Excel or with open-source alternatives such as OpenOffice.

Figure 5 - source data 1.

This spreadsheet contains the firing rate and spike count data for mitral cells used to generate the bar plots and average data shown in Figures 5C, 5D, and 5F. These data can be opened with Microsoft Excel or with open-source alternatives such as OpenOffice.

Figure 6 - source data 1.

This spreadsheet contains the firing rate and spike count data for mitral cells used to generate the bar plots and average data shown in Figures 6C, 6D, 6F, and 6H. These data can be opened with Microsoft Excel or with open-source alternatives such as OpenOffice.

Figure 7 - source data 1.

This spreadsheet contains the membrane potential data for mitral cells used to generate the bar plots and average data shown in Figures 7C and 7D. These data can be opened with Microsoft Excel or with open-source alternatives such as OpenOffice.

FIGURE 1

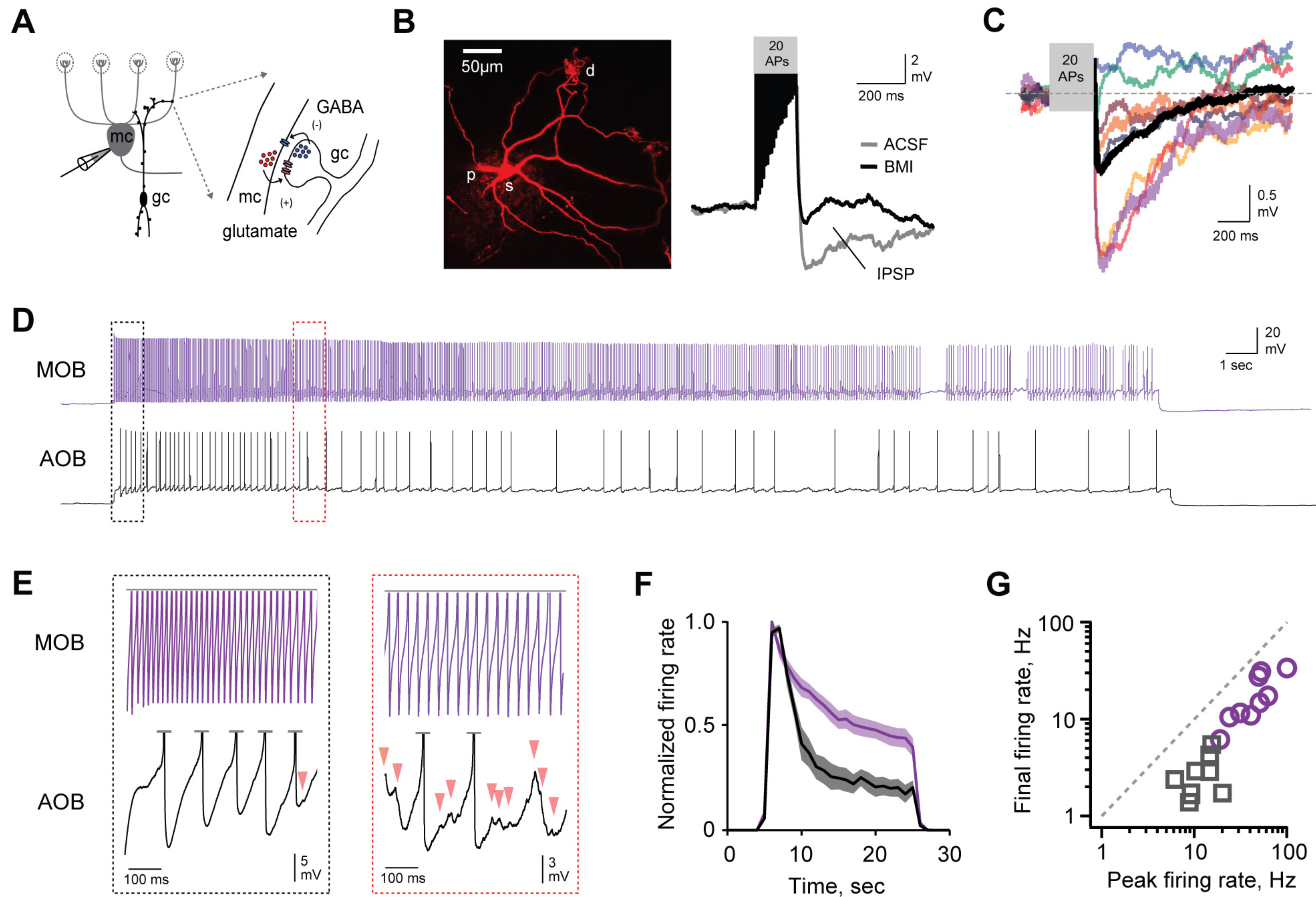


FIGURE 1 figure supplement 1

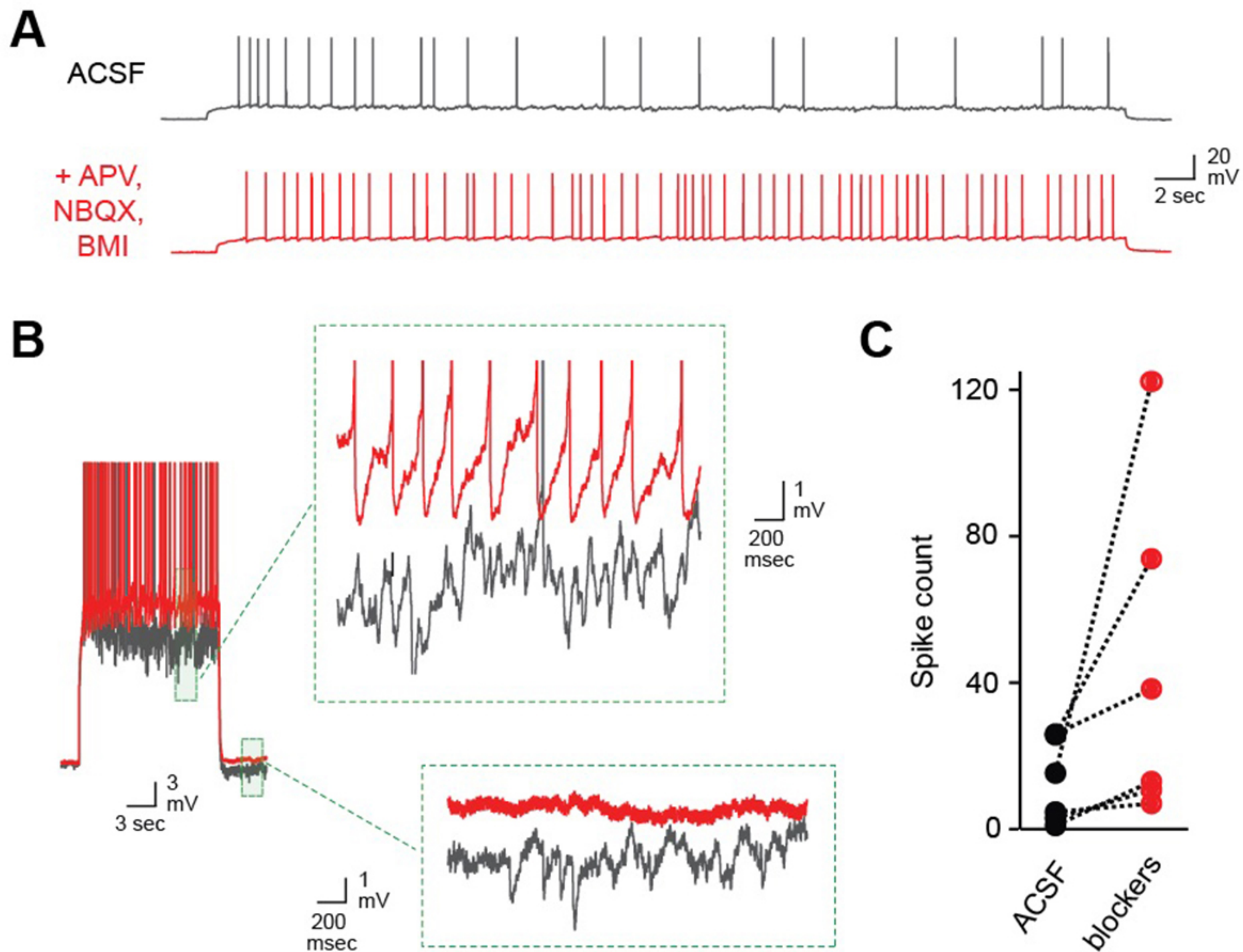


Figure 2

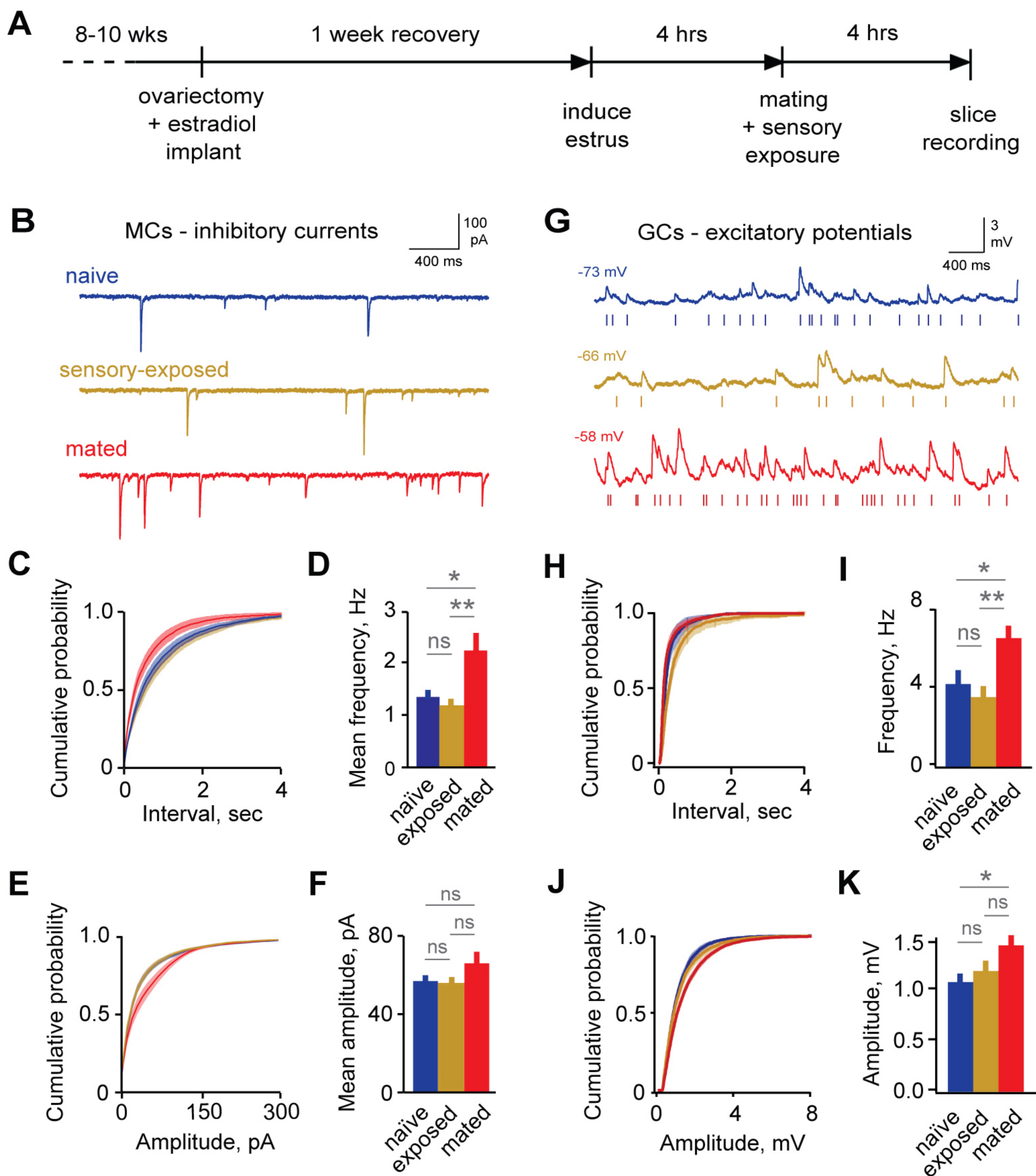


Figure 2 figure supplement 1

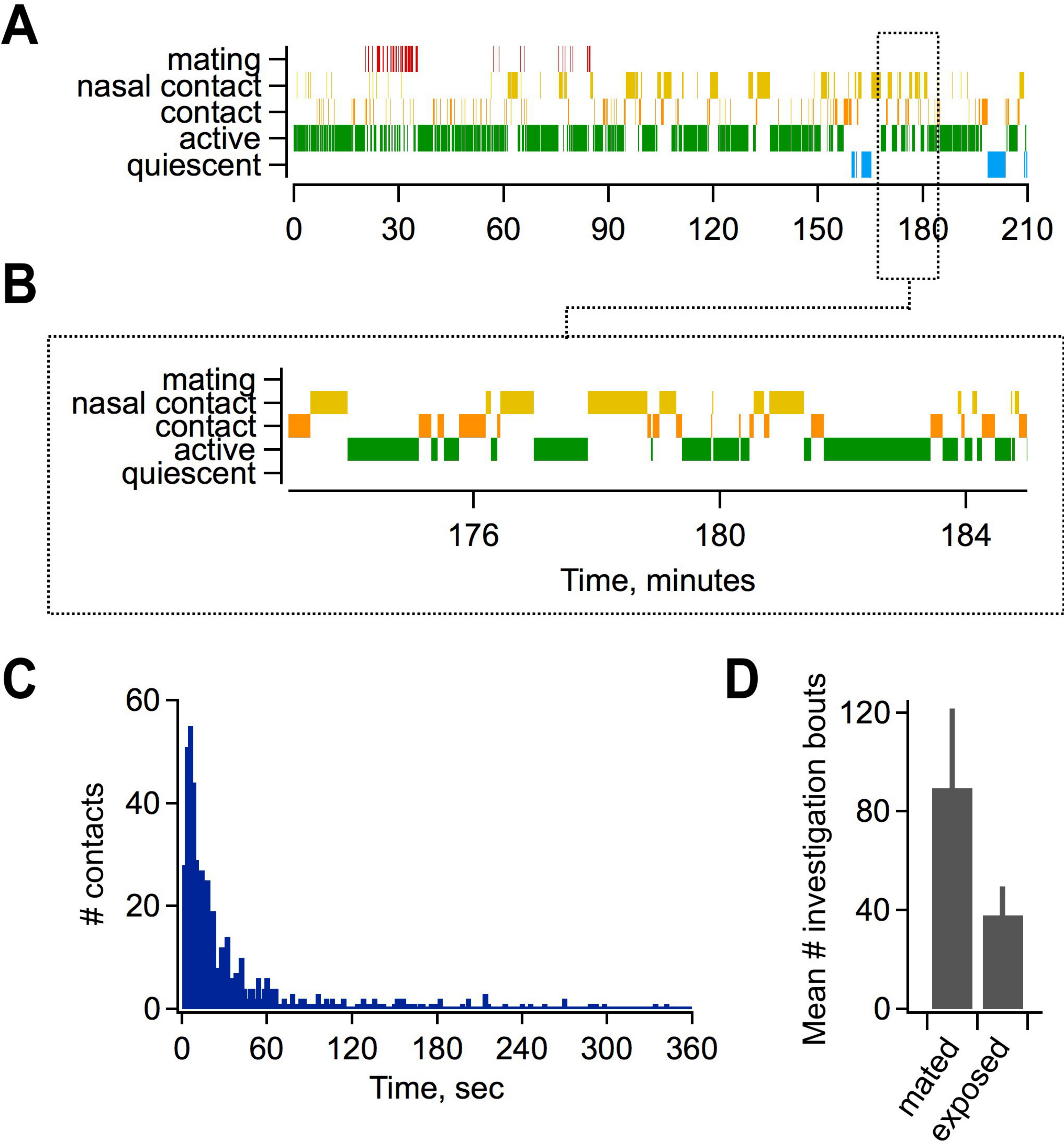


Figure 2 figure supplement 2

+ TTX, NBQX, APV



+ 15 μ M BMI

Figure 2 figure supplement 3

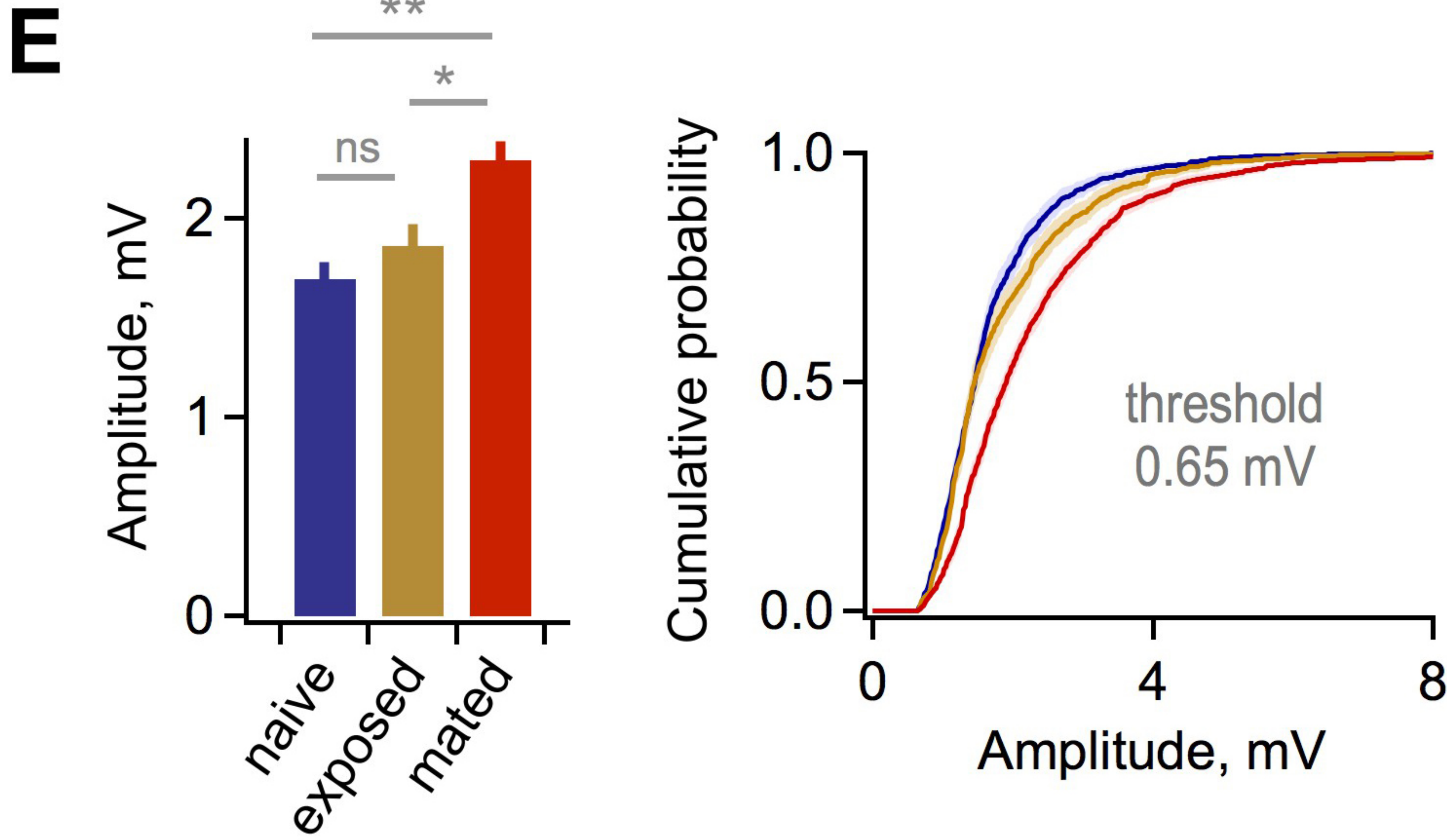
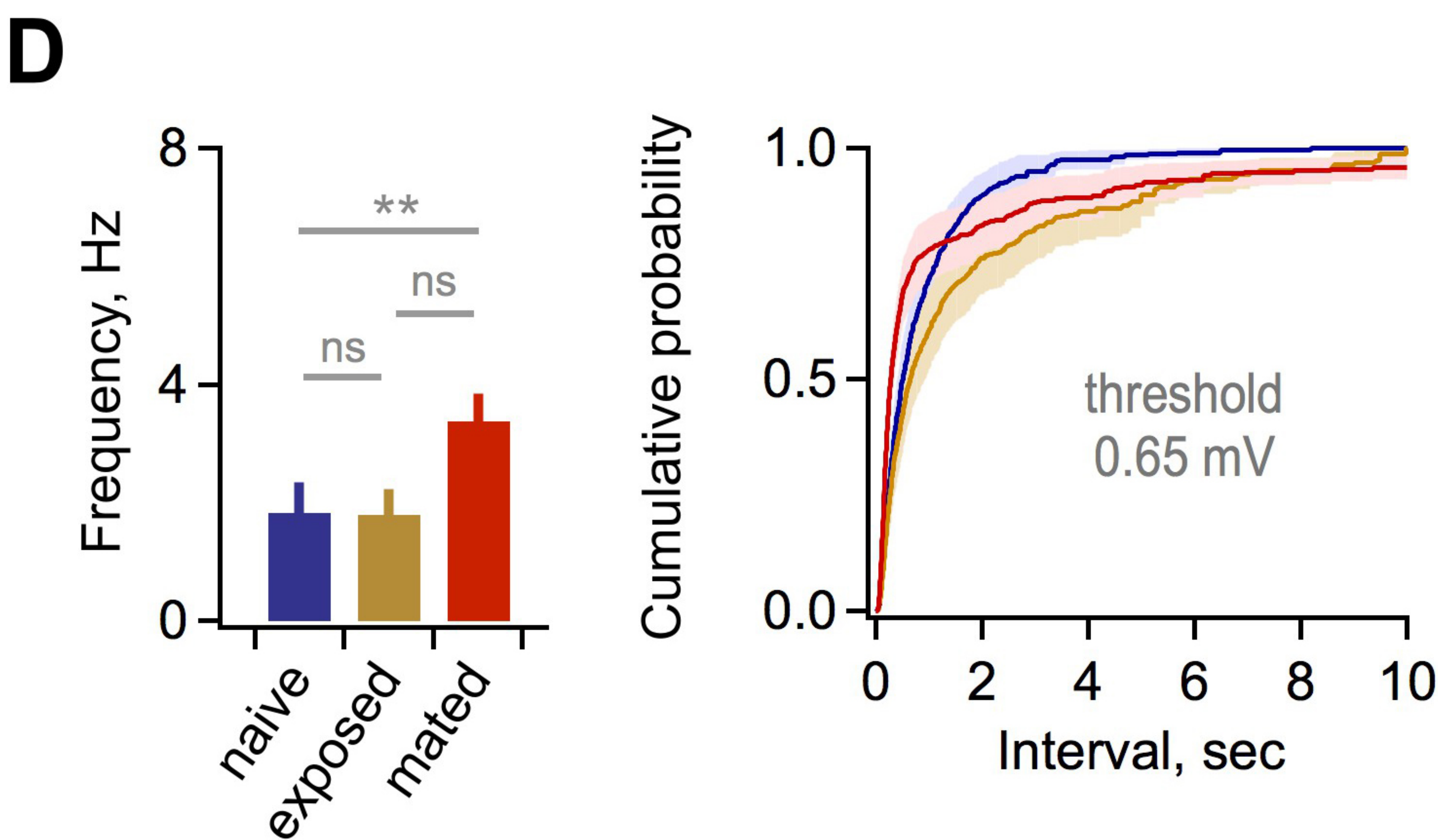
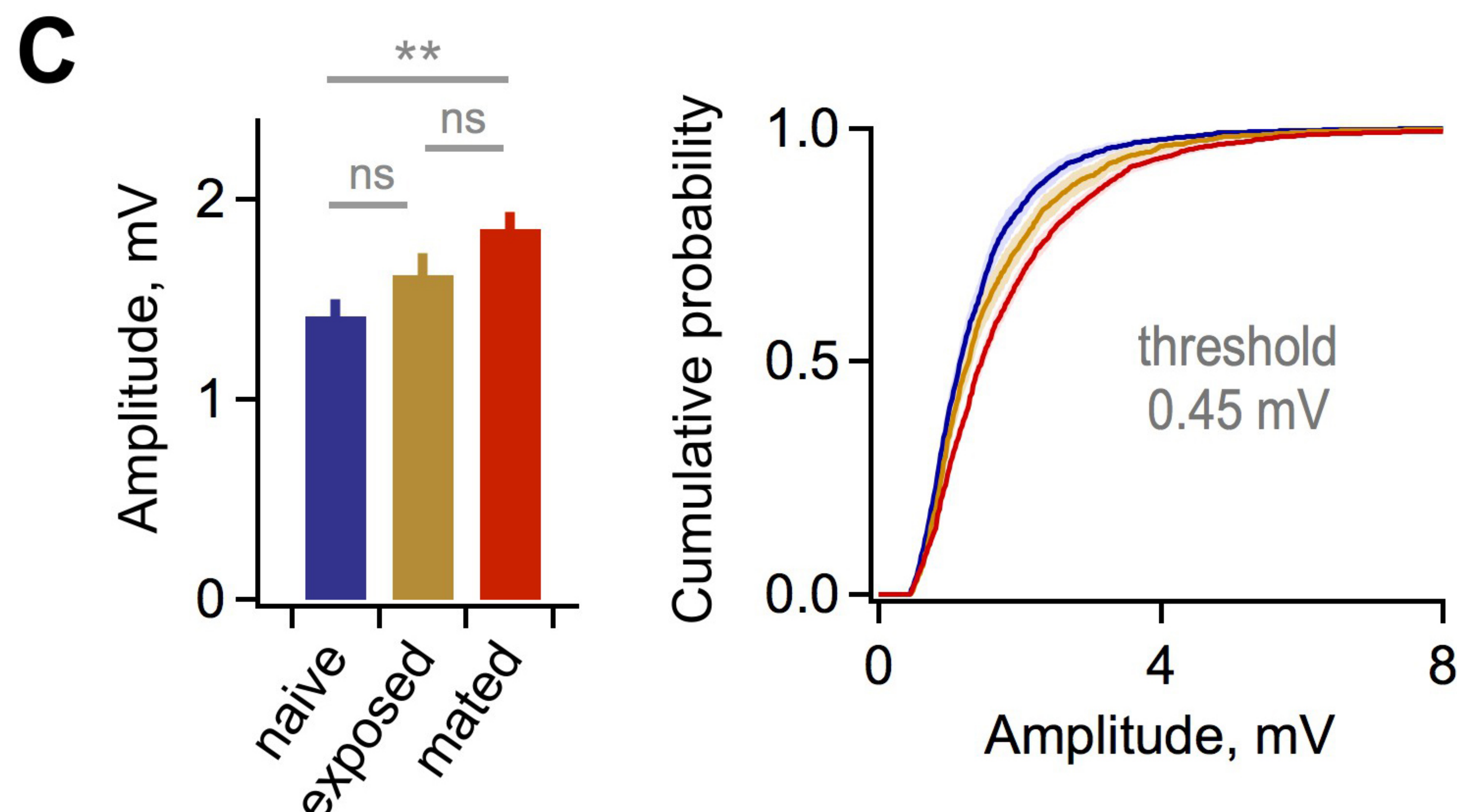
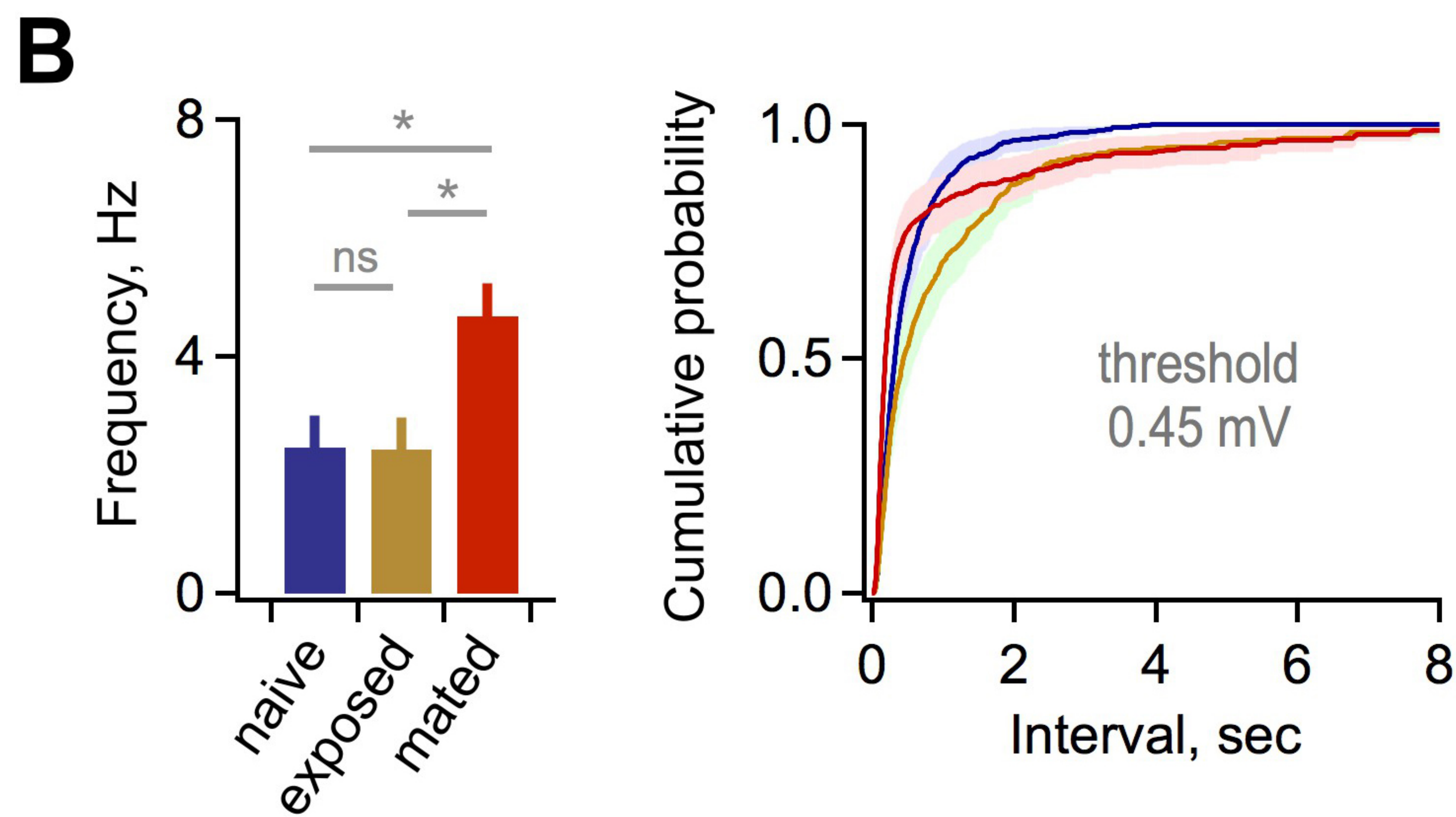
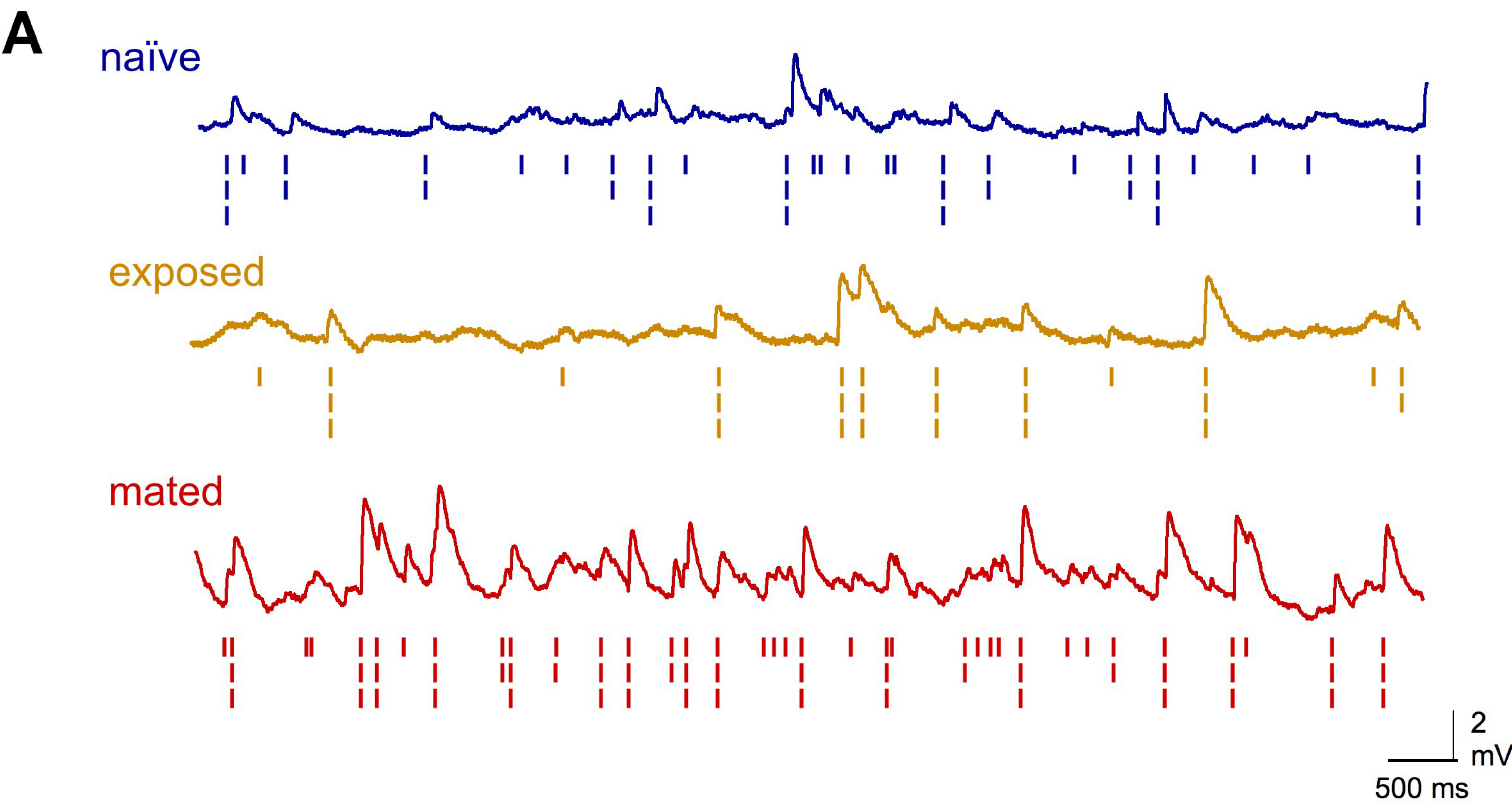


Figure 3

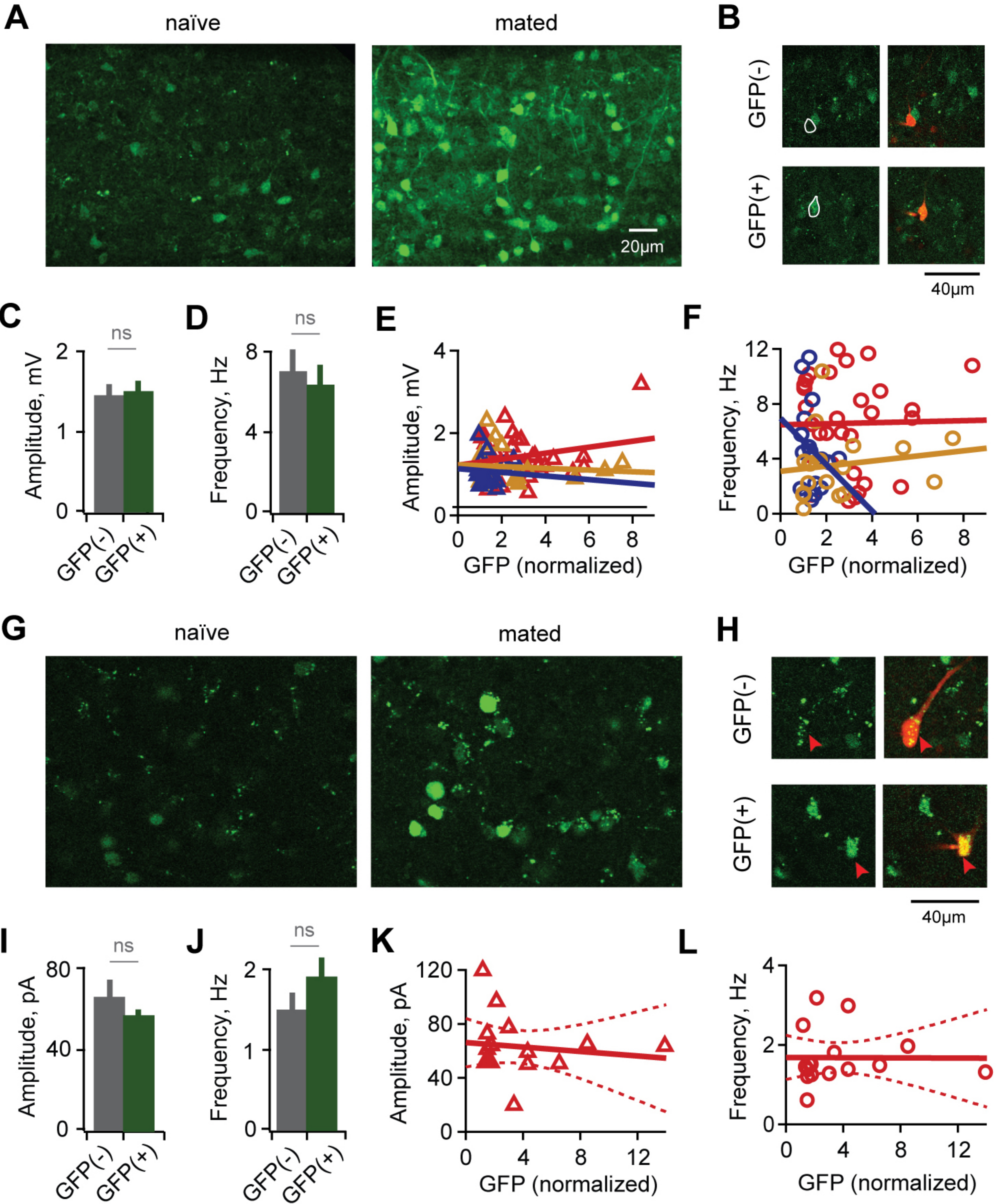


Figure 3 figure supplement 1

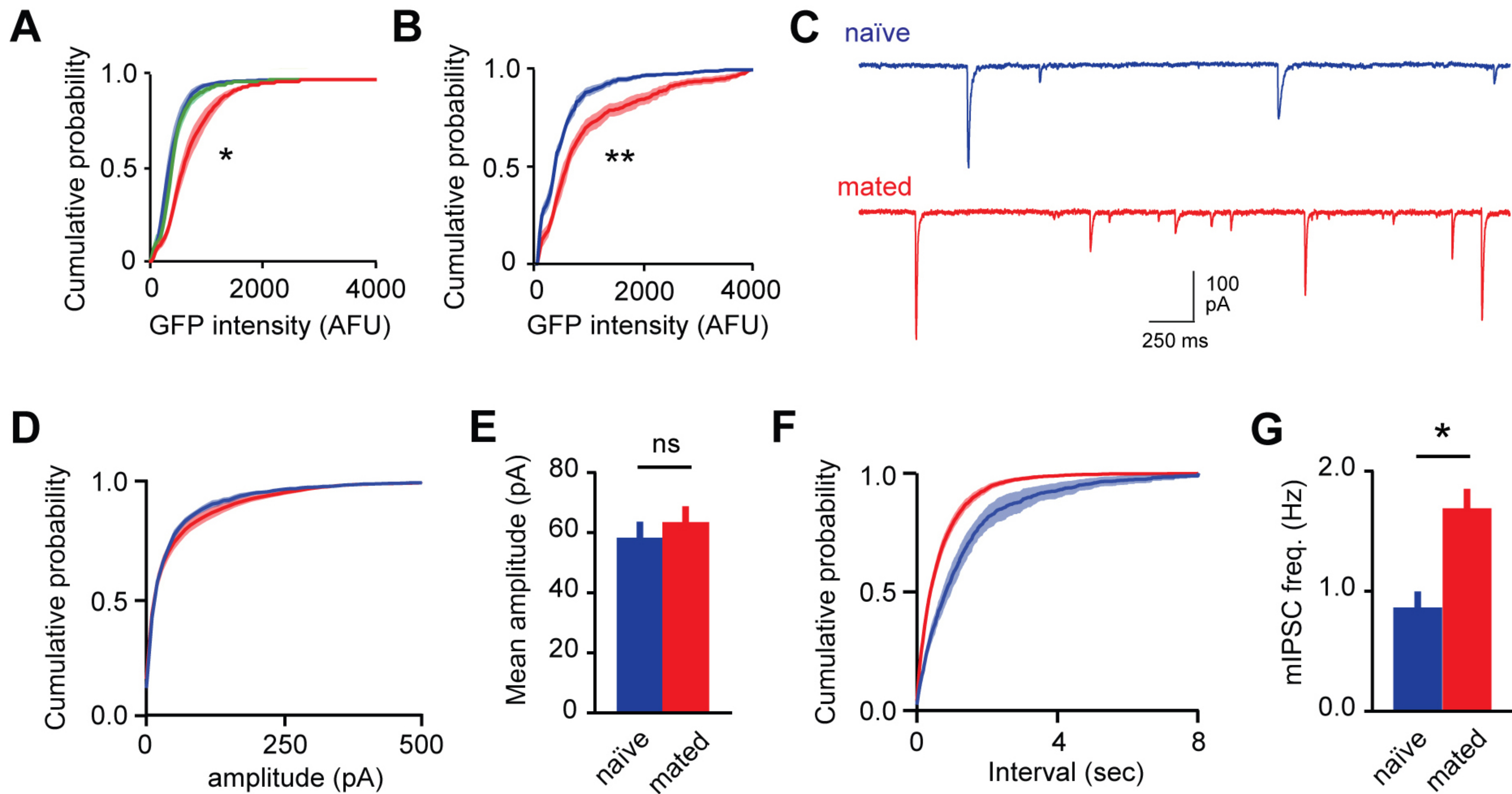


Figure 4

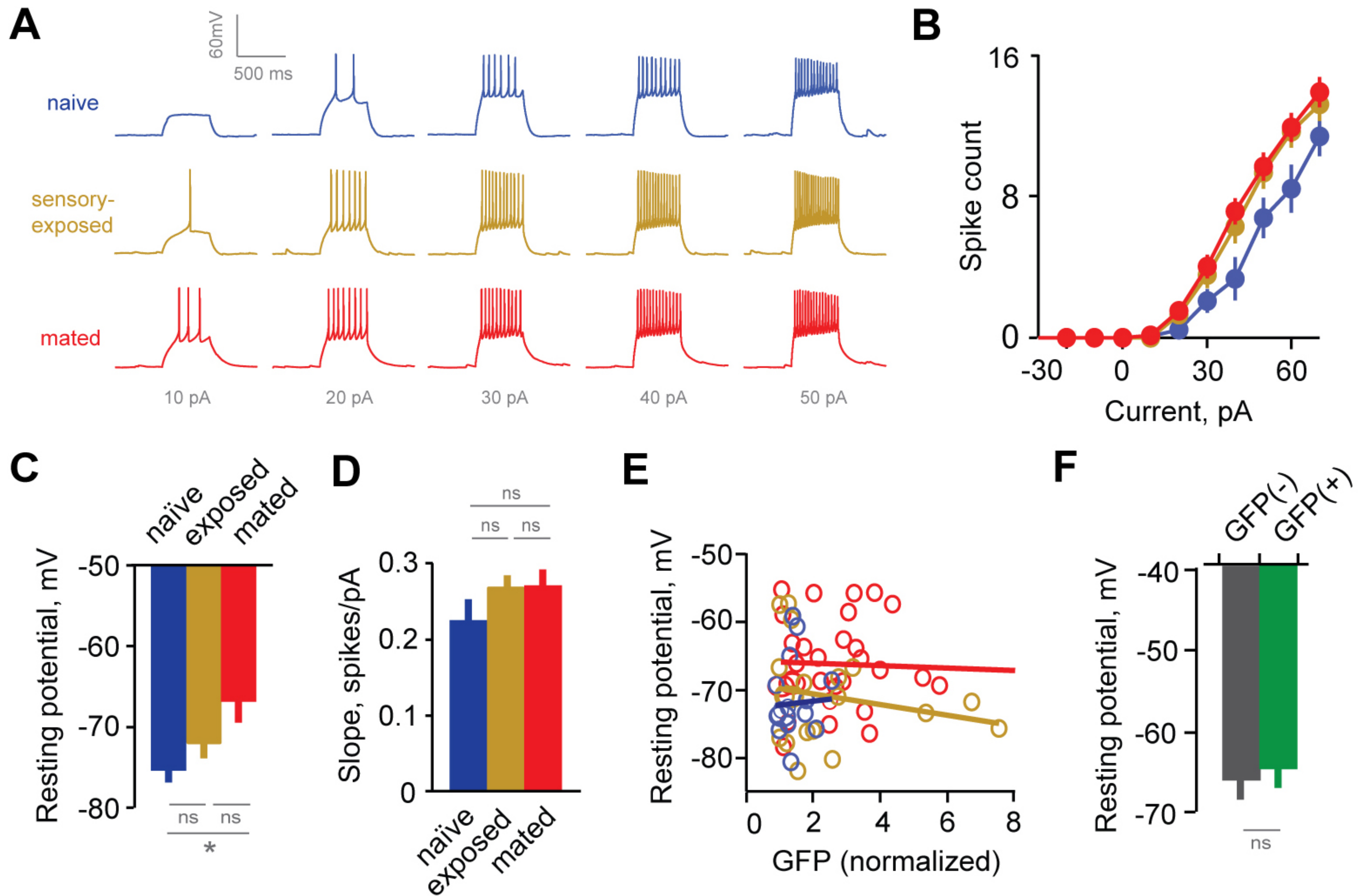


Figure 5

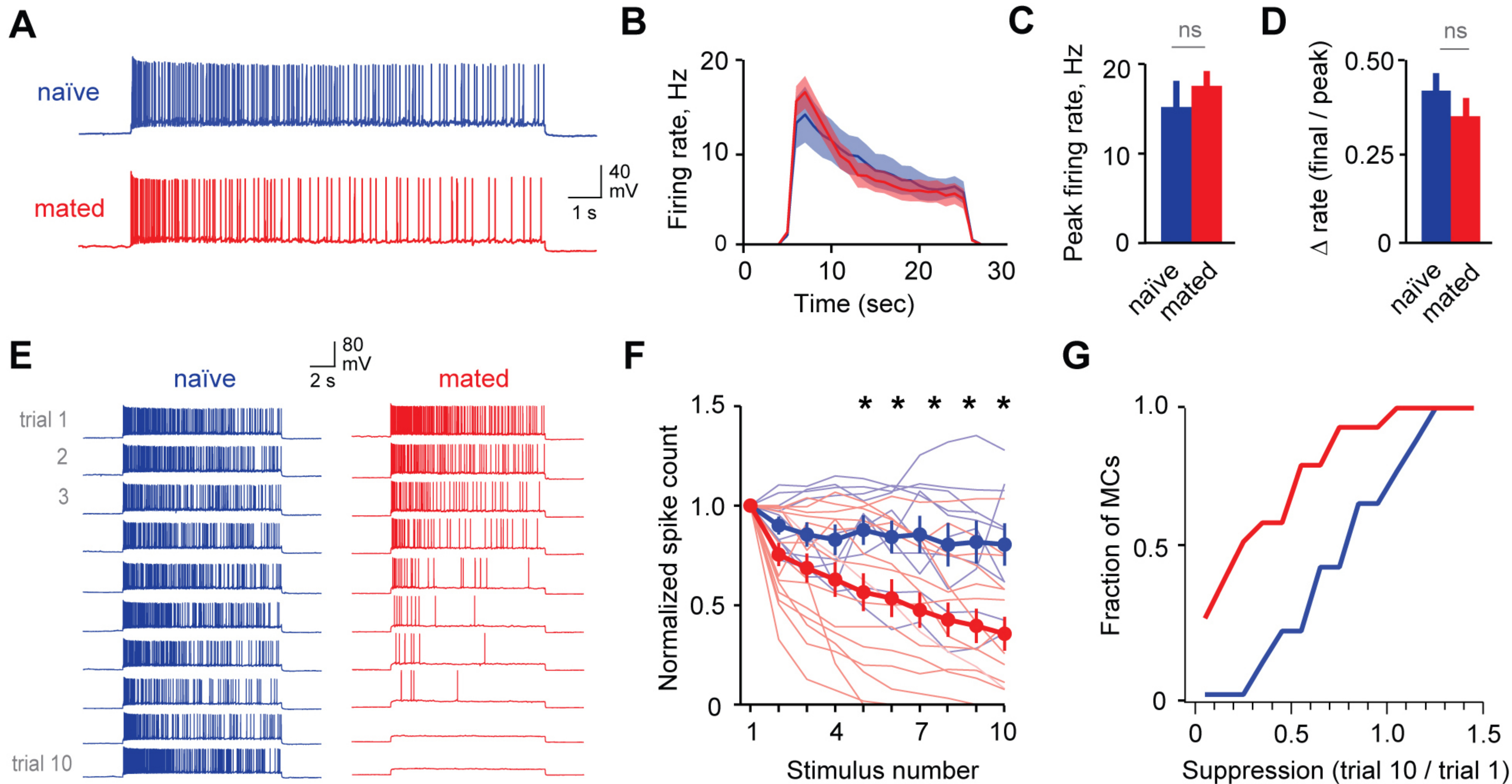


Figure 6

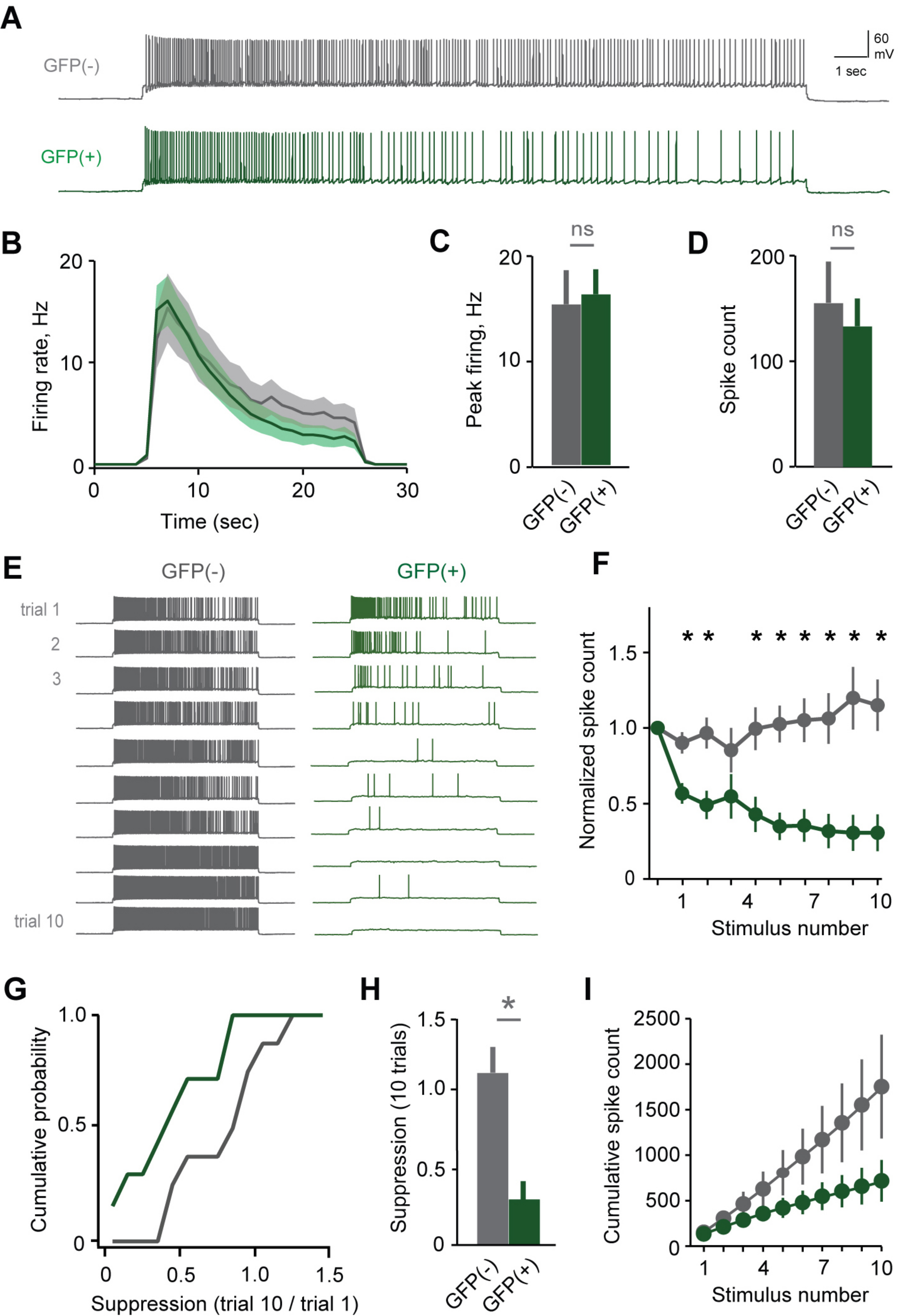


Figure 6 figure supplement 1

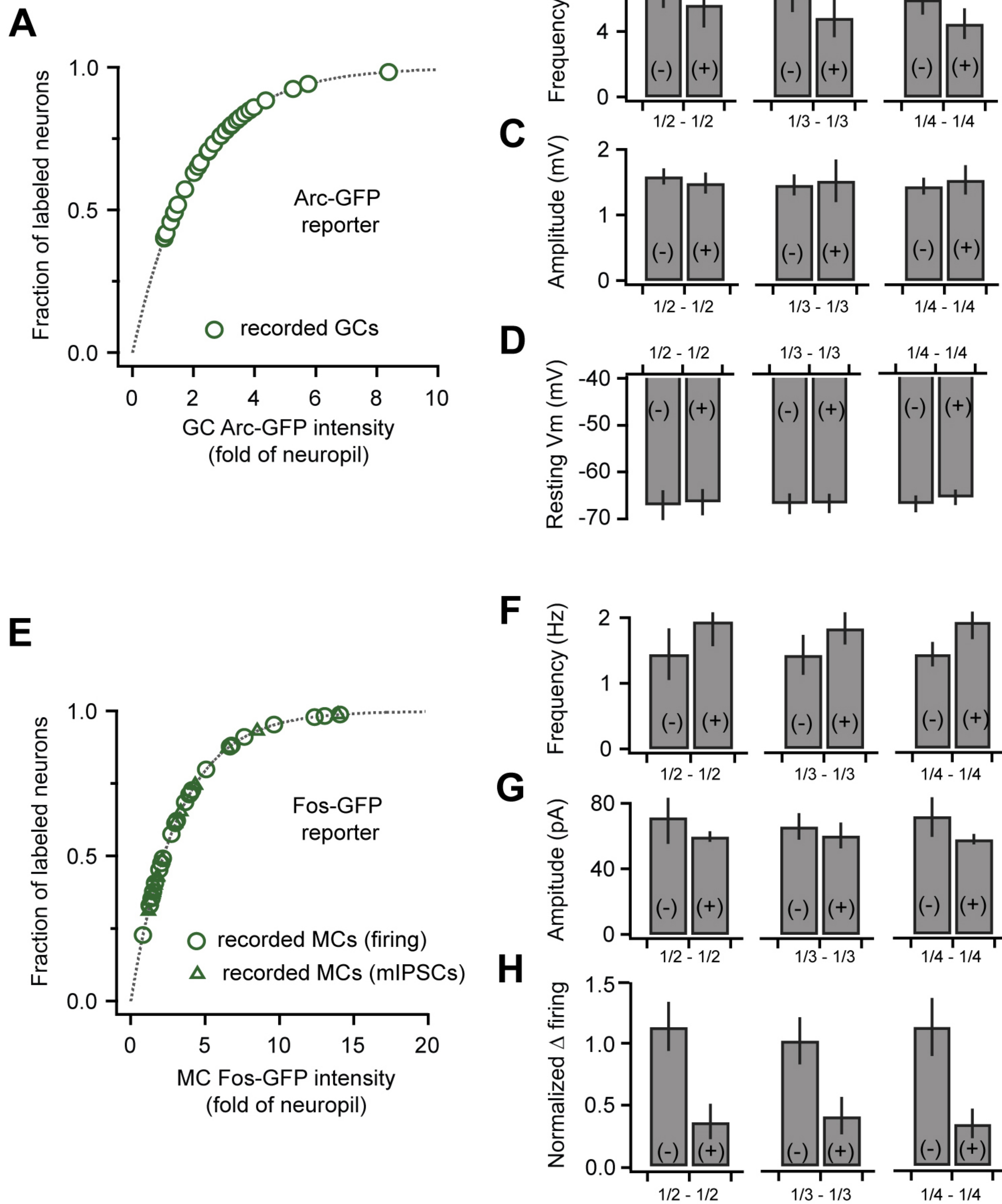


Figure 6 figure supplement 2

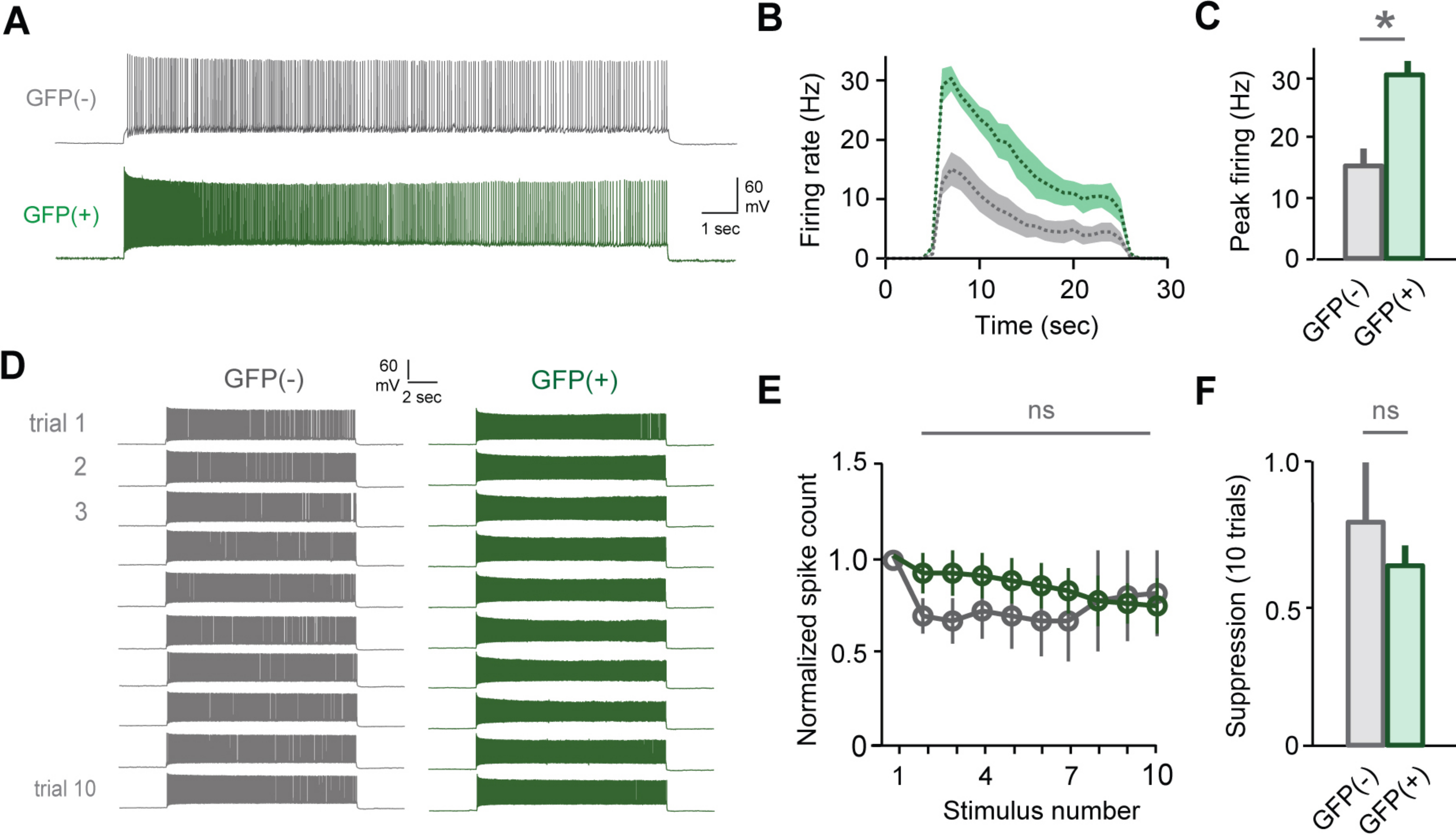


Figure 7

